Quarterly Journal of the Royal Meteorological Society
A journal of the atmospheric sciences and physical oceanography
RMetS

A high-impact meso-beta vortex in the Adriatic Sea

Journal:	*QJRMS*
Manuscript ID	QJ-22-0096.R1
Wiley - Manuscript type:	Research Article
Date Submitted by the Author:	n/a
Complete List of Authors:	Miglietta, Mario; ISAC-CNR Buscemi, Federico; Università degli Studi di Bologna Dafis, Stavros; National Observatory of Athens Papa, Alvise; Centro Previsione e Segnalazione Maree Tiesi, Alessandro; ISAC -CNR Conte, Dario; ISAC CNR Davolio, Silvio; ISAC-CNR Flaounas, Emmanouil; HCMR Levizzani, Vincenzo; ISAC-CNR Rotunno, Richard; NCAR
Keywords:	Dynamic/Processes < 1. Tools and methods, Extra-tropical weather systems < 6. Application/context, Mesoscale < 2. Scale, Severe weather < 3. Physical phenomenon, Mid-latitude < 5. Geographic/climatic zone, Atmosphere < 4. Geophysical sphere
Country Keywords:	Italy, Croatia

A high-impact meso-beta vortex in the Adriatic Sea

Mario Marcello Miglietta*, Federico Buscemi, Stavros Dafis, Alvise Papa, Alessandro Tiesi, Dario Conte, Silvio Davolio, Emmanouil Flaounas, Vincenzo Levizzani, Richard Rotunno

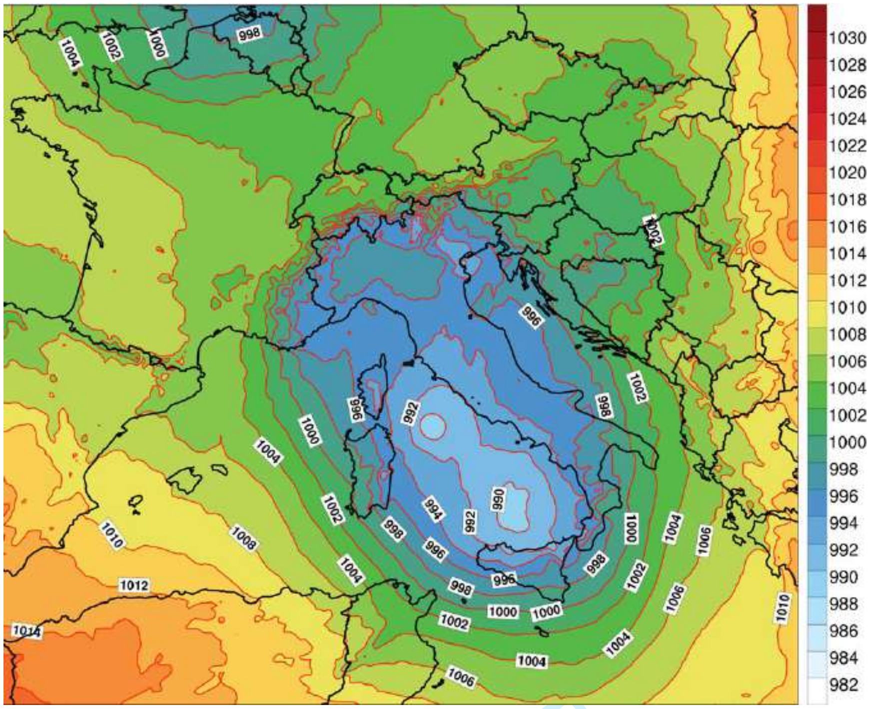

At about 2000 UTC, November 12, 2019, a small warm-core cyclone, formed in the central Adriatic Sea, made landfall near Venice and was responsible for an exceptional high tide. Convection and sea surface fluxes did not play a significant role in the cyclone development, notwithstanding its low-level warm core. Conversely, the interaction between the upper-level PV anomaly and the low-level baroclinicity was responsible for its intensification, in a manner similar to a transitory (stable) baroclinic interaction at small horizontal scales.

A high-impact meso-beta vortex in the Adriatic Sea

Mario Marcello Miglietta[1,*], Federico Buscemi[2,^], Stavros Dafis[3], Alvise Papa[4], Alessandro Tiesi[1], Dario Conte[1], Silvio Davolio[1], Emmanouil Flaounas[5], Vincenzo Levizzani[1], Richard Rotunno[6,°]

[1]National Research Council - Institute of Atmospheric Sciences and Climate (CNR-ISAC), Italy

[2]University of Bologna, Bologna, Italy

[3]National Observatory of Athens - Institute for Environmental Research and Sustainable Development (NOA/IERSD), Greece

[4]Centro Previsioni e Segnalazione Maree, Venice, Italy

[5]Institute of Oceanography, Hellenic Centre for Marine Research (HCMR), Athens, Greece

[6]NCAR°, Boulder, USA

^ (now at 3Bmeteo)

°The National Center for Atmospheric Research is sponsored by the National Science Foundation

* *Corresponding author address:* Mario Marcello Miglietta, CNR-ISAC, corso Stati Uniti 4, 35127 Padua, Italy.

E-mail: m.miglietta@isac.cnr.it

Keywords: cyclones; Mediterranean; potential vorticity; mesoscale; convection; severe weather; sea surface fluxes

Abstract

On the evening of November 12, 2019, an exceptional high tide – the second highest in the ranking since sea-level data have been recorded – hit the city of Venice in Northern Italy and its entire lagoon, damaging a large part of its historical center. A small warm-core mesoscale cyclone, which formed in the central Adriatic Sea and intensified during its northwestward movement toward the Venice lagoon, was responsible for the event. The cyclone was preceded by intense northeasterlies (Bora) in the northern Adriatic, which turned to southeasterlies (Sirocco) and then southwesterlies after its passage.

Simulations with different initialization times were carried out with the Weather Research and Forecasting (WRF) model. Simulation results show a strong sensitivity to the initial conditions, since the track (and strength) of the cyclone was determined by the exact position of an upper-level potential vorticity (PV) streamer. The factors responsible for the cyclone development and its characteristics are also investigated. The pre-existence of positive low-level cyclonic vorticity, associated with the convergence of the Sirocco and Bora winds in the central Adriatic, made the environment favorable for cyclone development. Also, the interaction between the upper-level PV anomaly and the low-level baroclinicity, created by the advection of warm, humid air associated with the Sirocco, was responsible for the cyclone's intensification, in a manner similar to a transitory (stable) baroclinic interaction at small horizontal scales. Sensitivity experiments reveal that convection, latent heat release and sea surface fluxes did not play a significant role, indicating that this cyclone did not show tropical-like characteristics, notwithstanding its low-level warm core. Thus, the warm-core feature appears mainly as a characteristic of the environment in which the cyclone developed rather than a consequence of diabatic processes. Lastly, the cyclone does not fall into any of the existing categories for Adriatic cyclones.

1. Introduction

The Mediterranean basin is one of the 'climate hotspots', where the intensity and/or frequency of intense weather events (e.g., strong winds, heavy precipitation, storm surges) is expected to increase (IPCC, 2021). The societal impact of such extremes and the possible implications of climate change have raised a renewed interest in the study of Mediterranean cyclones, both in the scientific community (Flaounas et al., 2022) and by the general public. Accurate predictions are needed several days in advance to prevent or at least to mitigate potential damage to people, property, and environment. On a longer time scale, the changes in cyclone location and intensity induced by global warming have important implications for long-term policy planning.

While most cyclones affecting the Mediterranean have extratropical characteristics, sub-synoptic, hybrid vortices, known as Medicanes or Mediterranean tropical-like cyclones, are occasionally observed in the Mediterranean (Emanuel, 2005; Miglietta, 2019). Although they are receiving increasing attention in the scientific literature, the mechanisms of development and intensification are not yet fully understood.

The intensification of Medicanes was shown to critically depend on sea surface temperature (SST; Miglietta et al., 2011; Pytharoulis, 2018; Noyelle et al., 2019), as it affects the strength of air-sea interaction processes and thus the thermal disequilibrium responsible for deep convection. However, baroclinic instability may cooperate for their development (Flaounas et al., 2021); thus, a classification was proposed, depending on the relative importance of baroclinic and diabatic processes during the mature stage (Miglietta and Rotunno, 2019; Dafis et al., 2020). The SST may play a secondary role in the development of very intense extratropical cyclones, which are governed by baroclinic instability, as the recent Vaia storm (Davolio et al., 2020). In all cases, upper-level dynamics control the cyclones' evolution, determining their track and predictability (Miglietta et al., 2017; Portmann et al., 2020). Mediterranean cyclones are also affected by the complex topography surrounding the basin: for example, the orography may play a key role in their genesis (Buzzi and Tibaldi, 1978; Alpert et al., 1999; Moscatello et al., 2008a; Buzzi et al., 2020), while the modulation by the rough coastline may affect their subsequent development (Rasmussen and Zick, 1987; Ricchi et al., 2019).

Within the category of Mediterranean cyclones, those developing in the Adriatic Sea show specific characteristics, such as a limited extent, due to the morphology of the basin (a narrow NW-SE stretch of sea roughly 200 km wide confined between the Apennines and the Dinaric Alps). From a climatological perspective, the northern Adriatic was identified as a region of high cyclonic activity (e.g., Campins et al. 2006), or even as a prominent area for explosive deepening in the cold season (Maheras et al., 2001). Horvath et al. (2008) identified four types of cyclones over the Adriatic Sea, each with peculiar characteristics and distinctive dynamical features:

- type A: connected with preexisting Genoa cyclones, they are the result of the Alpine lee cyclogenesis process (e.g., Buzzi et al., 2020);
- type B: developed *in situ* without connections with other preexisting cyclones; they develop either because of dynamical and thermal effects contributing to a low-level thermal anomaly in the northern Adriatic area (B-I type), or of lee cyclogenesis downwind of the central Apennines (B-II type), but with scales of motions much smaller than that in Alpine cyclogenesis;
- type AB: with mixed types A and B characteristics; this category includes cases where two cyclones coexist, in the Gulf of Genoa and in the northern Adriatic, respectively ("twin" or "eyeglass" cyclones); Brzovic (1999) indicates that the Adriatic twin is generated as a lee cyclone with respect to the Dinaric Alps;
- type C: cyclones of different origin moving from the Atlantic or from the western Mediterranean Sea (as in Ricchi et al., 2019), apart from the Gulf of Genoa (belonging to type A).

Therefore, most cyclones reach the Adriatic after crossing the Apennines from the west; the complex orography surrounding the basin and the presence of the sea may reduce their predictability.

On November 12, 2019, a small, but very intense Adriatic cyclone contributed to a high tide, exceptional for the conditions in which it occurred (Ferrarin et al., 2021), that flooded 85% of the city of Venice and affected its entire lagoon, causing major damage to the buildings. The high tide was the result of concurrent in-phase factors: the storm surge related to the meteorological forcing (the water in the northern Adriatic was pushed by the strong Sirocco and deflected westward by the Bora winds), the astronomic tide, the deep small-scale pressure minimum (inverse barometric effect), the very high sea level values over all of the Adriatic Sea in the days before the event, and – above all - the intense southwesterlies, that pushed water toward the lagoon and generated high waves following the passage of the small-scale cyclone. The highest sea level observed in Venice was 189 cm, the second highest ever recorded since 1872, the year in which data collection began, just 5 cm below the record reached on November 4, 1966. Unfortunately, operational weather models slightly underestimated the intensity of the cyclone and misplaced the track by some tens of kilometers, in most cases predicting its transit to the southwest of the lagoon, and not across it as it was observed (Bianco et al., 2020). Hence, considering the very specific location and topography of the affected regions and the small scale of the cyclone, current state-of-the-art models may be problematic in terms of flooding potential: even a slight misplacement may cause errors of several centimeters in the prediction of sea level height. The specific sensitivity of the region to even the smallest errors in the cyclone track/intensity requires additional guidance involving ocean metrics (as in Ferrarin et al., 2021).

The present paper aims at investigating the characteristics of the environment in which the cyclone developed, using an extensive set of surface observations and high-resolution numerical simulations. The paper is organized as follows: material and methods are reported in Section 2, synoptic analysis and surface data are described in Section 3, numerical simulation results are analyzed in Section 4, while the Discussion and Conclusions are in Section 5.

2. Material and Methods

The surface data analyzed in the present study were acquired from the integrated weather-tide networks of the Italian Institute for Environmental Protection and Research (ISPRA) and of the Tide Forecast and Early Warning Center of the city of Venice (CPSM). Also, the data from two weather-tide stations (*Piattaforma Acqua Alta CNR* and *Meda Abate*), belonging to the National Research Council - Institute of Marine Sciences (CNR-ISMAR), located offshore respectively at about 15 and 40 km from the Venetian coast, are analyzed. All these stations were installed to provide a detailed representation of the meteorological/marine conditions in the North Adriatic, with the purpose of improving the predictability of high tides that frequently affect Venice (Bianco et al., 2020).

A selection of weather stations was used in this work to better understand the evolution and the track of the cyclone (Fig. 1). These stations were selected to represent the atmospheric conditions in Venice (Palazzo Cavalli), in different lagoon subareas (Diga Sud Lido e Faro, Chioggia Porto, Malamocco Porto), in the open sea (Piattaforma CNR and Meda Abate) as well as far away from the lagoon, on its western (Padova Meteo) and southern side (Foce Po). The real-time data and the historical series of all the forty-two stations in the network are available online (www.venezia.isprambiente.it, www.comune.venezia.it/maree).

Numerical simulations were performed with the WRF-ARW model, version 4.0 (Skamarock et al., 2019) using three one-way nested domains (Fig. 2). The grids cover respectively the western Mediterranean (grid 1, horizontal spacing = 9 km, 250 × 220 grid points), northern and central Italy and most of the Adriatic regions (grid 2, horizontal spacing = 3 km, 382 × 235 grid points), the northern Adriatic Sea (grid 3, horizontal spacing = 1 km, 322 × 364 grid points); 41 vertical levels were employed. GFS analysis/forecasts (0.25° horizontal resolution) were used as initial and 3-hourly boundary conditions, respectively. The implementation in the "control" runs includes Thompson et al. (2008) microphysics, the Kain-Fritsch convection scheme (activated in the two outer domains; Kain, 2004), Mlawer et al. (1997) longwave radiation, Dudhia (1989) shortwave radiation, Noah land-surface model (Niu et al., 2011), and the Yonsei University boundary layer (YSU; Hong et al., 2006). The configuration is the one used for the simulations of an intense storm in the same region (Manzato et al., 2020), with the difference that the Thompson parameterization is preferred to the WSM5 scheme following the results of preliminary sensitivity tests. Additionally, the one-way nesting option produced more realistic results than the two-way nesting configuration and was therefore employed.

3. Synoptic conditions and surface data

On November 10, a wide trough in the middle troposphere elongated southward from the North Sea toward the western Mediterranean (Fig. 3a) and deepened due to the arrival of cold air. A surface cyclone, formed between Sardinia and the Balearic Islands at around 1200 UTC (Fig. 3a), shrank and strengthened in the following 12 hours (Fig. 3b). In the meantime, an upper-level pressure low appeared in the western Mediterranean. Then, its center moved over Algeria at 0000 UTC, November 11 (Fig. 3b), southwest of Tunisia at 1200 UTC (Fig. 3c) and approached again the Mediterranean Sea at around 0000 UTC, 12 November (Fig. 3d). On November 11, the surface cyclone moved southward and gradually weakened after landing over Algeria in the evening. Another surface cyclone moved from the leeward of the Atlas Mountains, where it originated, to the southern Mediterranean at around 1200 UTC (Fig. 3c), intensifying in the following 12 hours as it moved to Sicily (Fig. 3d). On November 12, the upper-level and the surface cyclones were almost aligned over the southern Tyrrhenian Sea, between Sicily, Sardinia, and Tunisia, and reached their maximum intensity (Fig. 3e). The slow evolution of the depression was favored by the presence of the Azores high to the west and an anticyclone over eastern Europe (Fig. 3e). Only in the evening the low weakened progressively as it moved toward the Tyrrhenian coast of southern Italy (Fig. 3f). Along the northeastern border of this large-scale cyclonic circulation, a weaker, smaller-scale pressure minimum formed over the Adriatic Sea at around 1200 UTC (Fig. 3e), and started moving northwestward, almost parallel to the Italian coast, reaching the Venice lagoon at around 2100 UTC (Fig. 3f).

Figure 4 shows the temporal evolution of the mean sea level pressure (mslp) at some selected stations. The rapid variation of the mslp values was associated with the passage of the small-scale cyclone, which produced a pressure drop of about 7 hPa in 3-4 hours at the stations near the cyclone track, while the recovery to the values preceding the passage of the cyclone was even faster. Because of the cyclone movement, a temporal delay of about 1.5 hour is apparent between the southern and the northernmost stations. The lowest pressure minimum (of about 987 hPa) was recorded at Piattaforma CNR, suggesting that the maximum intensity of the cyclone was probably reached over the open sea, just before it reached the lagoon.

Some indications on the precise track of the cyclone can be extracted from the overview of the observed wind fields at selected time steps (Fig. 5). At 1600 UTC, a moderate Bora wind blew over the lagoon, while the cyclone was still some hundred kilometers far south; at 1920 UTC, the approaching cyclone was revealed by easterly winds over the open sea and a progressive wind rotation in Foce Po to northwesterly and then to southwesterly at 2005 UTC, the latter associated also with an intensification of the wind speed. Thus, at 2005 UTC the observations indicate that the cyclone center was located on the north side of the Po Delta, close to the Adriatic coast. The wind barbs at 2040 and 2055 UTC identify a small-scale cyclonic circulation entering the lagoon from its southern part, where wind directions reversed over a distance of a few km; also, while intense southeasterlies blew over the open sea, sustained northeasterlies were still affecting the northern side of the lagoon.

Lastly, at 2125 UTC, as the cyclone moved inland, the wind rotated to southwesterly in the southern part of the lagoon and over the open sea, attaining its maximum intensity in response to the strong pressure gradient on the rear of the cyclone. Many stations in and around the lagoon (Fig. 6) recorded fierce winds up to 29 m s^{-1} in “Diga Sud Lido e Faro” station. The strong southwesterlies pushed the water toward the northern side of the lagoon, contributing to the extreme high tide. Following these considerations, the cyclone center is estimated to have remained close to the Adriatic coast along its entire track, landing just north of Chioggia (Fig. 1).

Figure 7 compares the evolution of different surface parameters at two selected stations, respectively over the open sea (Piattaforma CNR) and in Venice (Palazzo Cavalli). The measurements show an increase in the 2 m air and dewpoint temperature as the cyclone approached the stations: in Piattaforma CNR, a sudden increase of more than 4 K in 10 min preceded the arrival of the pressure minimum by about 50 minutes. During the next hour, the air temperature remained almost constant, decreasing rapidly 15 min after the passage of the minimum. The increase in dew point temperature was smaller, determining a reduction in relative humidity from saturation to 80%. At the Venice station a similar evolution was observed, but with a delay of 30 min; however, the temperature increase was less steep and mainly distributed in two distinct phases. After the passage of the cyclone, the environmental parameters went back to the previous values.

In conclusion, the presence of a low-level warm core (Fig. 7), the rapid change in wind speed near the center (Fig. 6), and the appearance of a cloud-free center in the visible satellite image (not shown) suggest a possible tropical-like nature of the cyclone, although the horizontal extent appears smaller than that recorded in any previous case (cfr. Miglietta et al., 2013). However, for a Medicane, which is mainly driven by air-sea interaction and latent heat release due to convection around the cyclone, the warm core is expected to be nearly symmetric and close to center. Figure 7 shows that in the present case the warm core preceded the arrival of the pressure minimum by about 1 hour and ended abruptly after its passage. Hence, considering these contrasting features, numerical simulations were performed to better clarify the nature (baroclinic versus tropical-like) of the cyclone.

4. Numerical simulations

4.1 Preliminary results

To investigate the predictability of the event and to understand the physical mechanisms responsible for the development of the cyclone, numerical simulations were carried out with the WRF-ARW model. A first intercomparison was performed among three model simulations starting at different initial times, i.e., 1200 UTC, November 11, 0000 and 1200 UTC, November 12 (hereafter named as run 1112, 1200, 1212, respectively). As described below, the cyclone track and intensity differed significantly among the simulations.

Figure 8a shows the time evolution of mslp simulated at the grid point closest to the Palazzo Cavalli weather station (Fig. 1). Only run 1212 is able to correctly reproduce the intensification of the cyclone in the late evening, although it underestimates the minimum by 4 hPa; in contrast, run 1112 precedes its occurrence by a few hours, while ERA5 reanalysis, and to a greater degree run 1200, strongly underestimate its deepening. Simulations performed with other models (BOLAM, COSMO-LAMI, ECMWF IFS) have similarly showed large uncertainties in reproducing the observed cyclone evolution (Bianco et al., 2020).

Similarly, the cyclone track (i.e., the line connecting the minimum mslp locations at different times) significantly differs among the numerical experiments. Figure 8b shows that only run 1212 correctly predicts the landfall on the southern side of the lagoon; the ERA-5 track is positioned to the west, and, consequently, precedes the observed landfall (over the Po Delta) by a few hours; run 1200 puts the cyclone track too far east, while run 1112 reproduces an intermediate track, which crosses the north side of the Venice lagoon. The limited predictability of the cyclone track can be also inferred from the ECMWF IFS runs issued 1-to-4 days earlier, which simulate an early landfall near the Po Delta only partially corrected in the later run initialized at 0000 UTC, 12 November (Cavaleri et al., 2020).

Another relevant aspect emerging from the simulations is the extremely weak sensitivity to grid spacing. For all experiments, the outputs on the three domains are nearly identical to each other; this result is somewhat unexpected considering the small dimensions of the cyclone, which should be better resolved at higher resolution. The archive of the operational runs performed with two limited area models developed at CNR-ISAC, i.e. BOLAM (Davolio et al., 2020; 8.3 km grid spacing) and MOLOCH (Malguzzi et al., 2006; Trini Castelli et al., 2020; 1.25 km grid spacing), available at https://www.isac.cnr.it/dinamica/projects/forecasts/, shows similar results, as the strength of the cyclone simulated with the coarser model (hydrostatic, convection parameterized) appears very similar or even slightly more intense than that obtained with the finer-scale model (nonhydrostatic, convection permitting). Similarly, Hallerstig et al. (2021) found that for four polar lows the difference in performance between the 9 km and 5 km versions of the ECMWF model, either with parameterized

257 or with explicit convection, was relatively small, especially for the two cyclones with baroclinic
258 characteristics (their Fig. 8). Following the hypothesis of Cioni et al. (2018) for a Mediterranean
259 tropical-like cyclone, that "simulations performed with a grid spacing larger than 5 km are not able
260 to correctly resolve the deep convection" and that convection "weakening or even absence
261 compromises the forecast of the cyclone evolution over time", and given the simulation results
262 described above, we speculate that latent heat release in convective cells does not play a relevant role
263 for the present case study. This conclusion is also supported by the negligible differences in cyclone
264 track and depth among simulations using a treatment of convection other than the control run (i.e.,
265 explicit convection either in the two inner grids or in all three grids; not shown).

266 Lastly, further numerical experiments were performed to test different model parameterization
267 schemes and domains (not shown). Sensitivity to these characteristics is significantly weaker than
268 that due to initial/boundary conditions (as discussed above) but is still responsible for changes in the
269 cyclone strength and track. These changes, although small from a meteorological point of view, may
270 yield problematic guidance in terms of flooding potential, having a strong effect on the simulation of
271 wave height and surge (Ferrarin et al., 2021). In fact, the impact of the latter in a small-scale basin
272 such as the Venice lagoon is strongly dependent on even minimal variations in meteorological
273 parameters and requires additional guidance in terms of ocean metrics.

274 ***4.2 Insight into the development mechanism***

275 The atmospheric conditions in which the cyclone developed are analyzed here using the run 1212 to
276 better understand the physical mechanisms responsible for its intensification. As discussed in Section
277 3, the cyclone appeared in the central Adriatic, in the lee of the Apennines, in the afternoon of
278 November 12, and then moved counterclockwise driven by the larger-scale cyclonic circulation
279 centered over the Tyrrhenian Sea. As a result of the latter, the Mistral developed over the western
280 Mediterranean basin, while intense Sirocco winds affected the southern and central Adriatic Sea, with
281 greater intensity on the eastern (Croatian) coast (Fig. 9). Meanwhile, the northern Adriatic was still

under the influence of northeasterly (Bora) wind, so that, at the border between the two circulations (Sirocco and Bora), strong low-level cyclonic vorticity (an ingredient favorable to the formation of Mediterranean cyclones; Cavicchia et al., 2014) developed over the central Adriatic before the appearance of the cyclone. Later, the Sirocco progressively strengthened and entered the northern Adriatic, so that the developing cyclone was advected northward by the southeasterly steering flow.

Figure 10 shows the 2D frontogenesis function (Petterssen, 1936), defined as the rate of change over time of the horizontal potential temperature gradient: $F = \frac{d}{dt}|\nabla_p \theta|$; here it is calculated at 950 hPa (the highest values are observed in the layer 1000-950 hPa) from the large-scale GFS data used to force the numerical simulations. As the warm environment in which the cyclone developed moved northward, the horizontal thermal gradient in the baroclinic zone on the northern side of the cyclone progressively increased.

The change in the thermal environment surrounding the cyclone can be identified in Fig. 11. A baroclinic zone appeared at the upper level in the afternoon, associated with the approach of cold air from the south that produced an increase in the thermal gradient in the layer 600-300 hPa (green contours). Conversely, a core of low-level warm air in the layer 1000-700 hPa (red contours) surrounded the mslp minimum, remaining confined around it at 20 UTC. Meanwhile, a tongue of low-level warm air moved from the central to the northern Adriatic coast in about 6 hours, as indicated by the northward movement of the 290 K isotherm at 1000 hPa (blue contours).

Consequently, in the low-levels the low-θ_e air in the northern Adriatic was progressively replaced by a high-θ_e air tongue carried by the Sirocco from the southern Adriatic Sea. A comparison of the low-level θ_e at different times in the three panels of Fig. 12 reveals the warm tongue progressively weakened as the air moved northward, due to the mixing with the surrounding low-θ_e air, which was transported over the northern Adriatic initially by the Bora and later by southwesterly winds from the Po valley on the rear side of the cyclone. In fact, the counterclockwise circulation associated with the small-scale cyclone advected the high-θ_e air to its front side, preceding the arrival of its center.

Meanwhile, on its rear, the outflow of cold/dry air from the eastern Po valley, generated by the evaporative cooling of the precipitation at the foot of the Apennines (as discussed in Section 3.2 of Ferrarin et al., 2021), interrupted the supply of warm and moist air from the south (Fig. 12c).

Therefore, the cyclone pressure center was not aligned with the low-level θ_e maximum, but lagged instead at its back, in an environment of strong horizontal thermal gradient, in accordance with the observed temporal shift between the arrival of warm air and the pressure minimum (Fig. 7). Considering the distribution and temporal evolution of θ_e, one may speculate that the warm air was not a consequence of diabatic processes associated with the cyclone (i.e., generated by the latent heat released by convection), but rather a characteristic of the environment in which the cyclone formed. This is consistent with the analysis of the simulations in Section 4.1, where convection was inferred to play only a marginal role in the development of the cyclone, and with the sensitivity experiments in Section 4.3.

To further illustrate this point, Figure 13 reports the vertical velocity at different levels (850, 700, 500 hPa) 1 hour before the cyclone reached its pressure minimum (2000 UTC). Only scattered and shallow convection was simulated, mainly confined below 5 km altitude. The most intense ascending motions appear in the Alpine area, due to the southerly flow over the orography (Fig. 13b), and near the Venice lagoon (Fig. 13c), at the northern and western end of the high-θ_e air tongue, where the warm air was raised above the pre-existent cold low-level air (in the region, the latter often act as an obstacle to the incoming moist and warm southerly flow; Davolio et al., 2016). Thus, the numerical simulations appear consistent with the sporadic lightning activity observed on the northwestern side of the cyclone before its landfall (https://www.blitzortung.org/en/historical_maps.php?map=10).

Finally, the contribution of the upper-level atmospheric features to the development of the cyclone is analyzed in Fig. 14, which shows the 300 hPa potential vorticity (PV) at 2000 UTC for the three runs. In both runs 1112 (Fig. 14a) and 1212 (Fig. 14c), the cyclone was positioned near an upper-level PV anomaly: in the first case, a secondary PV maximum was reproduced on the north side of the lagoon (the main streamer was positioned to the west), while in the latter, an intense PV streamer approached its southwestern part. In contrast, run 1200 (Fig. 14b) reproduced the PV anomaly inland, apparently unrelated to the position of the cyclone. Therefore, there are significant differences among the simulations in terms of intensity and exact position of the PV streamer. These results suggest that in run 1212 its position just above the observed cyclone location was critical to correctly reproduce the cyclone track: the PV anomaly was in correspondence with the left-exit of a jet stream that surrounded the synoptic cyclone (not shown), thus its location was favorable to the cyclone's intensification. Hence, we suppose that the upper-level dynamics played an important role for the evolution of the cyclone, and that were also fundamental for the correct prediction of the event, consistent with the results recently obtained for an intense Mediterranean cyclone (Portmann et al., 2020), although the scales involved here are much smaller. The role of the upper-level PV streamer and of its interaction with the warm and moist air advected in the low levels will be further discussed in the next Subsection.

4.3 Sensitivity experiments

To further investigate the mechanisms responsible for the intensification of the cyclone, a series of sensitivity experiments was undertaken. As in run 1212 (control run), the GFS analysis and forecasts initialized at 1200 UTC on 12 November were used as initial and boundary conditions. Only one domain (9 km horizontal spacing) was employed, considering the marginal effect of the resolution on the simulation results.

The sensitivity to different physical processes was explored in five numerical experiments:

1. NoSFFX: Full physics, but surface fluxes turned off.
2. NoLH: Full physics, but latent heat release turned off.
3. OnlyPBL: microphysics, radiation, and cumulus schemes turned off.

4. NoPhys: surface fluxes, latent heat release, and all physics parameterization schemes turned off.
5. NoPhysNoTopo: as NoPhys, but with terrain height = 1 m everywhere over land in the domain.

In all experiments 1-4, the track and landfall time were very close to those of the control run, so that the changes in the outputs can be considered as an effect of the physics and cannot be attributed to changes in the track.

In the NoSFFX run, the absence of surface fluxes caused a weakening of the small-scale minimum by about 2 hPa (Fig. 15a). However, the cyclone can still be identified near Venice (Fig. 15c), showing that the air-sea interaction processes, while participating in the cyclone intensification, were not fundamental for its occurrence and persistence. Likewise, surface fluxes only marginally affected the large-scale cyclone over the Tyrrhenian Sea.

In the NoLH run, the absence of latent heat release produced a substantial increase in mslp in all the areas affected by the large-scale cyclonic circulation covering the central Mediterranean basin, the strongest increase (greater than 4 hPa) being near the center of the Tyrrhenian cyclone (Fig. 15b). The Adriatic cyclone was only marginally affected, since the variation in mslp was only 1 hPa greater than in the surrounding areas, so that closed isobars can still be clearly identified around the mslp minimum (Fig. 15d). Hence, the NoLH run confirms that convection had a secondary effect on the small-scale cyclone. The two sensitivity experiments NoSFFX and NoLH indicate that the cyclone would persist even by removing air-sea interaction and convection, although the latter explain part of its intensification. In order to apply the "factor separation" technique (Stein and Alpert, 1993) and estimate the interaction of the two terms, an additional sensitivity experiment has been undertaken by removing simultaneously the surface fluxes and latent heat release, showing results very close to that of the NoLH run. This means that the small-scale cyclone had distinctive characteristics from

Mediterranean tropical-like cyclones, which, conversely, are mostly sustained by diabatic processes and a strong feedback between air-sea interaction and convection.

Even in the OnlyPBL run (microphysics, convection, and radiation switched off; boundary layer processes active) and in the NoPhys run (all parameterization schemes, sea surface fluxes and latent heat release switched off), the cyclone, albeit weaker, can still be identified near the Venice lagoon (Fig. 15e and 15f, respectively). Apparently, physics changed the cyclone evolution, but it was not required for its existence.

Lastly, a simulation without physics (as in the NoPhys run) and with flat orography (NoPhysNoTopo run) was performed. Even in this case, a closed minimum formed near the northern Adriatic Italian coasts, on the northern side of the trough axis extending from the large-scale minimum. The absence of orography apparently modified the location of the cyclone, which in this run was located inland, instead on the lee side of the Apennines, as observed. However, the presence of a small-scale minimum even without physics and orography (Fig. 16a) suggests that the large-scale forcing was the main driver for the development of the cyclone.

Using a diagnostic module implemented into the WRF model for the PV-budget (Flaounas et al., 2021), PV was calculated and decomposed into one conserved and several non-conserved partitions at each model time step. All these PV partitions are treated by the model as scalars, subject to advection. The adiabatic, conserved PV tracer (PVCO) represents the contribution of the large-scale flow and is only subject to advection. Conversely, non-conserved PV partitions are also subject to accumulations of gains/losses of PV, and derive from the net temperature and momentum forcings associated with the physical parameterization schemes. Overall, six non-conserved PV tracers are used, deriving from: latent heat release (microphysics and convection parameterizations); turbulent fluxes of temperature (boundary layer); atmospheric warming and cooling (shortwave and longwave radiation), and a momentum acceleration term (boundary layer). Details on how these terms are calculated can be found in Flaounas et al. (2021).

Positive values of PVCO appear close to the cyclone center before and around the time of its intensification (Fig. 16a). Figure 16b clarifies the interaction of the upper-level PV anomaly, associated with the lowering of the dynamic tropopause, with the baroclinicity at the side of the low-level warm tongue (i.e., high values of equivalent potential temperature), which was shifted westward with respect to the control run because of the suppression of the orography. Low values (below 10 K) of the coupling index (Bosart and Lackmann, 1995), around the area of cyclone development (central Adriatic) at 12 UTC and over the region of its maximum intensification (Venice lagoon) at 18 UTC, indicate the presence of conditions favorable to the interaction between positive upper-tropospheric and lower-tropospheric PV anomalies around the cyclone location (not shown).

Also, these results suggest some analogies with the mechanism theoretically described in Rotunno and Fantini (1989, their Fig. 2), i.e. a transitory (stable) baroclinic interaction. In this kind of development, a surface cyclone forms and deepens when a pre-existing upper-level trough encounters a low-level baroclinic zone (Petterssen's Type-B extra-tropical cyclones; Petterssen and Smebye, 1971) even for wavelengths shorter than that required for instability, since the system is capable of extracting energy from the mean flow.

4.4 Surface pressure tendency

To further investigate the atmospheric processes that contributed to the deepening of the cyclone, we used an additional diagnostic, i.e., the surface pressure p_{sfc} tendency equation (Fink et al., 2012):

$$\frac{\partial p_{sfc}}{\partial t} = DF + ITT + EP + RES \qquad (1)$$

where:

$DF = \rho_{sfc}\frac{\partial \phi_{p_2}}{\partial t}$ is the contribution due to the changes of the geopotential height ϕ at p_2 (ρ_{sfc}: air density at the surface), $EP = g\,(E - P)$ is the contribution of the change in water vapor mass due to evaporation E and precipitation P (g: gravitational acceleration), $ITT = \rho_{sfc} R_d \int_{sfc}^{p_2} \frac{\partial T_v}{\partial t} d\ln p$ is the vertically integrated virtual temperature T_v tendency (R_d: gas constant for dry air), and RES is the residual term due to numerical discretization. The equation was applied to a vertical column from the surface to the upper boundary $p_2 = 50\ hPa$ as in Fita and Flaounas (2018).

ITT can be further decomposed into:

$$ITT = TADV + VMT + DIAB + RES \quad (2),$$

where: $TADV = \rho_{sfc} R_d \int_{sfc}^{p_2} -\vec{\boldsymbol{v}} \cdot \nabla_p T_v d\ln p$ is the contribution of the horizontal virtual temperature advection ($\vec{\boldsymbol{v}}$ is the horizontal wind), $VMT = \rho_{sfc} R_d \int_{sfc}^{p_2} (\frac{R_d T_v}{c_p p} - \frac{\partial T_v}{\partial p}) \omega d\ln p$ is the contribution of the vertical motion (c_p is the specific heat capacity at constant pressure p; ω the vertical wind component in isobaric coordinates), $DIAB = \rho_{sfc} R_d \int_{sfc}^{p_2} \frac{T_v Q}{c_p T} d\ln p = TBL + THD + TLW + TSW$ represents the rate of change of temperature due to diabatic processes calculated by the WRF physical parameterizations (Q is the diabatic heating, TBL planetary boundary layer-related processes, THD microphysics and convective processes including latent heat release, TLW longwave radiation, and TSW shortwave radiation).

Integration was performed every 30 minutes over a circle of 100 km radius centered at the position of the surface cyclone; hence, due to the progressively smaller cyclone size, the area-average p_{sfc} remained nearly constant or slightly increased (rates less than 1 hPa 1 h^{-1}), although the minimum mslp progressively decreased as the cyclone approached Venice. All terms with time tendencies were calculated as area- or volume-averaged changes in 30 minutes, while the instantaneous terms TADV and VMT were computed by integration over the volume and then averaged over the time interval.

Figure 17a shows the different contributions to the equation and the total pressure tendency. The contribution of evaporation/precipitation EP appears marginal, while the geopotential change DF at the upper boundary is mainly responsible for a decrease of p_{sfc} at the time the PV streamer wrapped around the cyclone and the dynamic tropopause lowered just above its center (from about 1830 to 2000 UTC in the control run).

451 Figure 17b shows the different contributions to the *ITT* term. Although a comprehensive
452 interpretation is not possible due to the non-negligible residual, some considerations can be drawn:

453 - THD is very small during the cyclone intensification, confirming that microphysical processes
454 (e.g., latent heat release) play a marginal role in its evolution;

455 - TADV is always negative, which is indicative of warm advection associated with the
456 northward transport of warm air from the southern Mediterranean;

457 - TSW and TBL provide almost no contribution;

458 - TLW represents a small positive contribution (diabatic cooling);

459 - VMT is always positive and can be attributed to the large-scale ascent associated with the
460 lifting of the warm air advected from the south over the cold air pre-existent in the low levels
461 in the northern Adriatic Sea.

462 These results appear consistent with those emerging from the sensitivity experiments and in the
463 previous subsections and are indicative of the high influence of synoptic-scale dynamics on the
464 cyclone evolution.

465 **5. Discussion and Conclusions**

466 The present paper describes the unusual Mediterranean cyclone that affected the Venice lagoon on
467 12 November 2019. Although the skill of the real-time weather forecasts was generally acceptable
468 from a meteorological perspective (cyclone track missed by few tens of km and depth underestimated
469 by few hPa), the fine details necessary for impact applications were missed; consequently, the
470 operational prediction of the storm surge peak was underestimated by some tens of cm,
471 misrepresenting the severity of the tide that unexpectedly flooded most of the town, with dramatic
472 consequences in terms of costs and impact to human activities. Here, the event is re-analyzed from a
473 meteorological perspective, to understand the mechanism(s) of development of the small-scale
474 cyclone that was responsible for the extreme tide.

Numerical simulations performed with the WRF model, using three nested domains, show a strong sensitivity to the initial conditions: over the three full-physics simulations starting at different initial times, only the one starting closer to the occurrence of the cyclone shows an excellent agreement with the observed track, although it slightly underestimates the strength of the cyclone. The high-resolution inner domain, which explicitly resolves convection, does not improve the simulation results compared to the coarsest domain that uses parameterized convection; a similar behavior was reported in the numerical simulations performed for the same case with other meteorological models. This unexpected result is a consequence of the scattered and shallow convection simulated by the model, which has a negligible impact on the intensification of the cyclone.

The strong PV advection in the upper levels, combined with a pre-existing relative vorticity maximum (associated with the confluence of the Sirocco with the Bora wind) and the advection of warm and moist air in the lower levels, appear as the main factors responsible for the strong intensification of the cyclone in the northern Adriatic. In particular, the interaction of the upper-level (adiabatic) PV anomaly with the low-level baroclinic zone recalls a transitory (stable) baroclinic interaction at small horizontal scales.

The cyclone analyzed in the present work shows peculiar characteristics, which do not exactly fit into any of the categories proposed in Horvath et al. (2008) for Adriatic cyclones. Like category B-II cyclones, it has a small scale and originates downwind of the central Apennines; however, its movement along the Adriatic coast and its strong intensity differ from the typical characteristics of B-II cyclones (see Figure 3 in Horvath et al., 2008). As type-AB cyclones, it is characterized by the simultaneous presence of a large-scale cyclone, belonging to the same upper-level system, on its western side; however, it differs since the large-scale cyclone does not form over the gulf of Genoa (it originates in the lee of the Atlas Mountains) and both cyclones do not move southeastward along the Tyrrhenian coast and the Adriatic Sea respectively (they move northward, driven by a southerly steering flow). Finally, like category C-II cyclones, the large-scale system does not originate over the Adriatic and over the Gulf of Genoa, but it differs since the small-scale pressure minimum detaches from the large-scale cyclone (the presence of two simultaneous cyclones is not contemplated in the C-II category).

Sensitivity experiments indicate that sea surface fluxes were not important for the intensification of the cyclone. The secondary role played by the air-sea interaction processes and by convection indicate that the cyclone, even if it has a low-level warm core (its vertical extent can be estimated from 1000 to about 650 hPa), shows very different dynamics compared with Mediterranean tropical-like cyclones or with intense Mediterranean extratropical cyclones partially sustained by intense convection (e.g., Vaia storm; Davolio et al., 2020). Furthermore, the cyclone appears different from vortices in which the warm core is the result of seclusion of warm air (as described in Mazza et al., 2017; Fita and Flaounas, 2018; Category B in the classification of Miglietta and Rotunno, 2019 or Group 3 in the classification of Dafis et al., 2020); in fact, the cyclone develops at the southern tip of the warm and moist air tongue advected northward from the southern Mediterranean, several hundred km distant from the large-scale cyclone center, thus it is not associated with pre-existent baroclinic zones related to this larger-scale vortex. Some analogies can be found with Medicanes of Category C (Miglietta and Rotunno, 2019), such as the Ionian cyclone of September 2006 (Moscatello et al., 2008b), which showed a similar extent of a few tens of km and underwent a strong intensification after its interaction with an upper-level PV streamer associated with a large-scale pressure minimum over the Tyrrhenian Sea, as it moved near the left exit of a jet stream (Chaboureau et al., 2012). However, in contrast to the latter, the present cyclone did not exhibit a deep warm core, but rather hybrid characteristics.

In conclusion, the present study reaffirms the existence of a continuum of cyclones between tropical and extratropical systems, showing how the complex orography and rough coastline of the Mediterranean basin make the range of possible characteristics of cyclones even wider compared to environments with more uniform morphology. As suggested in Garde et al. (2010), a strong effort should be put in the numerical exploration of the gray areas between these two categories of cyclones, especially considering that the region is highly responsive to climate change (Giorgi, 2006), and that the risk related to Mediterranean cyclones is expected to increase in the future (e.g., Romera et al., 2017). This is especially true in the northern Adriatic, where a projected increase between 5 and 10 cm is expected in 100-year return times for Medicane-induced coastal sea-surface elevations, with significant inter-model agreement (Toomey et al., 2022). It is right along this line that the COST Action CA19109 "MedCyclones" has been trying to gather scientists of weather and climate, as well as the operational meteorological community, with the aim of improving our understanding of Mediterranean cyclones and attaining more accurate forecasts. The collaboration within the present research activity is a clear example of the powerful impact of sharing tools and expertise.

Acknowledgments

This work was supported by: the Technical-scientific Collaboration Agreement of CNR-ISAC with the Tide Forecast and Early Warning Center (CPSM) – Civil Protection - Municipality of Venice. The computational time was partially granted from the National Infrastructures for Research and Technology S.A. (GRNET S.A.) in the Greek HPC facility – ARIS under project adapt2CC. This article is a contribution to the COST Action CA19109 "MedCyclones: European Network for Mediterranean Cyclones in weather and climate".

REFERENCES

Alpert, P., Tsidulko, M. and Izigsohn, D. (1999) A shallow short-lived meso-beta cyclone over the Gulf of Antalya, eastern Mediterranean. Tellus A, 51, 249–262. https://doi.org/10.3402/tellusa.v51i2.12319

Bianco, A., Bonometto, A., Casaioli, M., Coraci, E., Cornello, M., Crosato, F., Ferla, M., Mariani, S., Morucci, S., Favaro, M., Massaro, G., Papa, A., Pastore, F., Sambo, E., Tosoni, A., Bajo, M., Cavaleri, L., Chiggiato, J., Ferrarin, C. and Umgiesser, G. (2020) Novembre 2019. Un mese di maree eccezionali. Dinamica e anomalie dell'evento del 12 novembre 2019. Dati, statistiche e analisi degli eventi. [A month of exceptional tides. Dynamics and anomalies of the event of 12 November 2019. Data, statistics and analysis of events]. Available at:

https://www.comune.venezia.it/sites/comune.venezia.it/files/documenti/centro_maree/bibliografia/Novembre_2019_un_mese_di_maree_eccezionali-Dinamica_e_anomalia_dell’evento_del_12novembre.pdf (Accessed: 18 March 2022)

Bosart, L. F. and Lackmann, G. M. (1995) Postlandfall tropical cyclone reintensification in a weakly baroclinic environment: A case study of Hurricane David (September 1979). Mon. Wea. Rev., 123, 3268–3291. doi:10.1175/1520-0493(1995)123<3268:PTCRIA>2.0.CO;2.

Brzović, N. (1999) Factors affecting the Adriatic cyclone and associated windstorms. Contrib. Atmos. Phys., 72, 51–65.

Buzzi, A. and Tibaldi, S. (1978) Cyclogenesis in the lee of the Alps: A case study. Quart. J. Roy. Meteor. Soc., 104, 271–287. https://doi.org/10.1002/qj.49710444004

Buzzi, A., Davolio, S. and Fantini, M. (2020) Cyclogenesis in the lee of the Alps: a review of theories. Bull. of Atmos. Sci. and Technol., 1, 433-457. https://doi.org/10.1007/s42865-020-00021-6

Campins, J., Jansà, A. and Genovés, A. (2006) Three-dimensional structure of western Mediterranean cyclones. Int. J. Climatol., 26, 323–343. https://doi.org/10.1002/joc.1275

Cavaleri, L., Bajo, M., Barbariol, F., Bastianini, M., Benetazzo, A., Bertotti, L., Chiggiato, J., Ferrarin, C., Trincardi, F. and Umgiesser, G. (2020) The 2019 flooding of Venice and its implications for future predictions. Oceanography, 33, 42-49. https://doi.org/10.5670/oceanog.2020.105

Cavicchia, L., von Storch, H. and Gualdi, S. (2014) A long-term climatology of medicanes. Clim. Dyn., 43, 1183–1195. https://doi.org/10.1007/s00382-013-1893-7

Chaboureau, J.-P., Pantillon, F., Lambert, D., Richard, E. and Claud, C. (2012) Tropical transition of a Mediterranean storm by jet crossing. Quart. J. Roy. Meteor. Soc., 138, 596–611. https://doi.org/10.1002/qj.960.

Cioni, G., Cerrai, D. and Klocke, D. (2018) Investigating the predictability of a Mediterranean tropical-like cyclone using a storm-resolving model. Quart. J. Roy. Meteor. Soc., 144, 1598–1610. https://doi.org/10.1002/qj.3322.

Dafis, S., Claud, C., Kotroni, V., Lagouvardos, K. and Rysman, J.-F. (2020) Insight into convective evolution of Mediterranean tropical-like cyclones. Quart. J. Roy. Meteor. Soc., 146, 4147–4169. https://doi.org/10.1002/qj.3896.

Davolio, S., Volontè, A., Manzato, A., Pucillo, A., Cicogna, A. and Ferrario, M. E. (2016) Mechanisms producing different precipitation patterns over North-Eastern Italy: insights from HyMeX-SOP1 and previous events. Quart. J. Roy. Meteor. Soc., 142, 188–205. https://doi.org/10.1002/qj.2731.

Davolio, S., Della Fera, S., Laviola, S., Miglietta, M.M. and Levizzani, V. (2020) Heavy precipitation over Italy from the Mediterranean storm "Vaia" in October 2018: Assessing the role of an atmospheric river. Mon. Wea. Rev., 148, 3571–3588. https://doi.org/10.1175/MWR-D-20-0021.1

Dudhia, J. (1989) Numerical study of convection observed during the winter monsoon experiment using a mesoscale two-dimensional model. J Atmos. Sci., 46, 3077–3107. https://doi.org/10.1175/1520-0469(1989)046<3077:NSOCOD>2.0.CO;2

Emanuel, K. (2005) Genesis and maintenance of Mediterranean hurricanes. Adv. Geosci., 2, 217–220. https://doi.org/10.5194/adgeo-2-217-2005

Ferrarin, C., Bajo, M., Benetazzo, A., Cavaleri, L., Chiggiato, J., Davison, S., Davolio, S., Lionello, P., Orlić, M. and Umgiesser, G. (2021) Local and large-scale controls of the exceptional Venice floods of November 2019. Progr. Oceanography, 197, 102628, https://doi.org/10.1016/j.pocean.2021.102628.

Fink, A.H., Pohle, S., Pinto, J.G. and Knippertz, P. (2012) Diagnosing the influence of diabatic processes on the explosive deepening of extratropical cyclones. Geophys. Res. Lett., 39, L07803, https://doi.org/10.1029/2012GL051025

Fita, L. and Flaounas, E. (2018) Medicanes as subtropical cyclones: the December 2005 case from the perspective of surface pressure tendency diagnostics and atmospheric water budget. Quart. J. Roy. Meteor. Soc., 144, 1028–1044, https://doi.org/10.1002/qj.3273

Flaounas, E., Gray, S.L. and Teubler, F. (2021) A process-based anatomy of Mediterranean cyclones: from baroclinic lows to tropical-like systems. Weather Clim. Dynam., 2, 255–279, https://doi.org/10.5194/wcd-2-255-2021.

Flaounas, E., Davolio, S., Raveh-Rubin, S., Pantillon, F., Miglietta, M.M., Gaertner, M.A., Hatzaki, M., Homar, V., Khodayar, S., Korres, G., Kotroni, V., Kushta, J., Reale, M. and Ricard, D. (2022) Mediterranean cyclones: current knowledge and open questions on dynamics, prediction, climatology and impacts. Wea. Clim. Dynam., 3, 173–208, https://doi.org/10.5194/wcd-3-173-2022.

Garde, L.A., Pezza, A.B. and Bye, J.A.T. (2010) Tropical transition of the 2001 Australian duck. Mon. Wea. Rev., 138, 2038–2057. https://doi.org/10.1175/2009MWR3220.1

Giorgi, F. (2006) Climate change hot-spots. Geophys. Res. Lett., 33, L08707, https://doi.org/10.1029/2006GL025734

Hallerstig, M., Magnusson, L., Kolstad, E.W. and Mayer, S. (2021) How grid-spacing and convection representation affected the wind speed forecasts of four polar lows. Quart. J. Roy. Meteor. Soc., 147, 150–165. https://doi.org/10.1002/qj.3911

Hong, S.-Y., Noh, Y. and Dudhia, J. (2006) A new vertical diffusion package with an explicit treatment of entrainment processes. Mon. Wea. Rev., 134, 2318–2341. https://doi.org/10.1175/MWR3199.1.

Horvath, K., Lin, Y.-L. and Ivančan-Picek, B. (2008) Classification of cyclone tracks over the Apennines and the Adriatic Sea. Mon. Wea. Rev., 136, 2210-2227. https://doi.org/10.1175/2007MWR2231.1

IPCC (2021) Climate Change 2021: The Physical Science Basis. Contribution of Working Group I to the Sixth Assessment Report of the Intergovernmental Panel on Climate Change, edited by: Masson-Delmotte, V., Zhai, P., Pirani, A., Connors, S. L., Péan, C., Berger, S., Caud, N., Chen, Y., Goldfarb, L., Gomis, M. I., Huang, M., Leitzell, K., Lonnoy, E., Matthews, J. B. R., Maycock, T. K., Waterfield, T., Yelekçi, O., Yu, R., and Zhou, B., Cambridge University Press.

Kain, J.S. (2004) The Kain-Fritsch convective parameterization: an update. J. Appl. Meteor., 43, 170–181. https://doi.org/10.1175/1520-0450(2004)043<0170:TKCPAU>2.0.CO;2

Maheras, P., Flocas, H.A., Patrikas, I. and Anagnostopoulou, C. (2001) A 40-year objective climatology of surface cyclones in the Mediterranean region: Spatial and temporal distribution. Int. J. Climatol., 21, 109–130. https://doi.org/10.1002/joc.599

Manzato, A., Riva, V., Tiesi, A. and Miglietta, M.M. (2020) Analysis of the 4 July 2007 hailstorm in NE Italy, Q. J. Roy. Meteor. Soc., 146, 3587-3611, 2020, https://doi.org/10.1002/qj.3886

Malguzzi, P., Grossi, G., Buzzi, A., Ranzi, R., and Buizza, R. (2006). The 1966 'century' flood in Italy: a meteorological and hydrological revisitation. J. Geophys. Res., 111, D24106, https://doi.org/10.1029/2006JD007111.

Mazza, E., Ulbrich, U. and Klein, R. (2017) The Tropical Transition of the October 1996 Medicane in the Western Mediterranean Sea: A Warm Seclusion Event. Mon. Wea. Rev., 145, 2575–2595. https://doi.org/10.1175/MWR-D-16-0474.1.

Miglietta, M.M., Moscatello, A., Conte, D., Mannarini, G., Lacorata, G. and Rotunno, R. (2011) Numerical analysis of a Mediterranean hurricane over south-eastern Italy: sensitivity experiments to sea surface temperature. Atmos. Res., 101, 412–426. https://doi.org/10.1016/j.atmosres.2011.04.006.

Miglietta, M.M., Laviola, S., Malvaldi, A., Conte, D., Levizzani, V. and Price, C. (2013) Analysis of tropical-like cyclones over the Mediterranean Sea through a combined modelling and satellite approach. Geophys. Res. Lett., 40, 2400–2405. https://doi.org/10.1002/grl.50432.

Miglietta, M.M., Cerrai, D., Laviola, S., Cattani, E. and Levizzani, V. (2017) Potential vorticity patterns inMediterranean “hurricanes”. Geophys. Res. Lett., 44, 2537–2545. https://doi.org/10.1002/2017GL072670.

Miglietta, M. M. (2019) Mediterranean tropical-like cyclones (Medicanes). Atmosphere, 10, 206.

Miglietta, M.M. and Rotunno, R. (2019) Development mechanisms for Mediterranean tropical-like cyclones (Medicanes). Quart. J. Roy. Meteor. Soc., 145, 1444–1460. https://doi.org/10.1002/qj.3503.

Mlawer, E.J., Taubman, S.J., Brown, P.D., Iacono, M.J. and Clough, S.A. (1997) Radiative transfer for inhomogeneous atmosphere: RRTM, a validated correlated k-model for the longwave. J. Geophys. Res., 102, 16663–16682. https://doi.org/10.1029/97JD00237.

Moscatello, A., Miglietta, M.M. and Rotunno, R. (2008a) Numerical analysis of a Mediterranean

657 "hurricane" over southeastern Italy. Mon. Wea. Rev., 136, 4373–4397.
658 https://doi.org/10.1175/2008MWR2512.1.
659 Moscatello, A., Miglietta, M.M. and Rotunno, R. (2008b) Observational analysis of a Mediterranean
660 'hurricane' over south-eastern Italy. Weather, 63, 306–311. https://doi.org/10.1002/wea.231
661 Niu, G.-Y. and Coauthors (2011) The community Noah land surface model with multi
662 parameterization options (Noah-MP): 1. Model description and evaluation with local-scale
663 measurements. J. Geophys. Res., 116, D1210. https://doi.org/10.1029/2010JD015139
664 Noyelle, R., Ulbrich, U., Becker, N. and Meredith, E.P. (2019) Assessing the impact of sea surface
665 temperatures on a simulated medicane using ensemble simulations. Nat. Hazards Earth Syst. Sci., 19,
666 941– 955. https://doi.org/10.5194/nhess-19-941-2019
667 Petterssen, S. and Smebye, S.J. (1971) On the development of extratropical cyclones. Quart. J. Roy.
668 Meteor. Soc., 97, 457-482.
669 Petterssen, S. (1936) Contribution to the theory of frontogenesis. Geof. Pub., 11(6), 1-27.
670 Portmann, R., González-Alemán, J.J., Sprenger, M. and Wernli, H. (2020) How an uncertain short-
671 wave perturbation on the North Atlantic wave guide affects the forecast of an intense Mediterranean
672 cyclone (Medicane Zorbas). Wea. Clim. Dynam., 1, 597–615. https://doi.org/10.5194/wcd-1-597-
673 2020.
674 Pytharoulis, I. (2018) Analysis of a Mediterranean tropical-like cyclone and its sensitivity to the sea
675 surface temperatures. Atmos. Res., 208, 167–179. https://doi.org/10.1016/j.atmosres.2017.08.009
676 Rasmussen, E. and Zick, C. (1987) A subsynoptic vortex over the Mediterranean with some
677 resemblance to polar lows. Tellus A, 39, 408–425. https://doi.org/10.1111/j.1600-
678 0870.1987.tb00318.x.
679 Ricchi, A., Miglietta, M.M., Bonaldo, D., Cioni, G., Rizza, U. and Carniel, S. (2019) Multi-physics
680 ensemble versus atmosphere-ocean coupled model simulations for a tropical-like cyclone in the
681 Mediterranean Sea. Atmosphere, 10(4), 202. https://doi.org/10.3390/atmos10040202.
682 Romera, R., Sanchez, E., Dominguez, M., Gaertner, M.A. and Miglietta, M.M. (2017) Climate

change projections of medicanes with a large multi-model ensemble of regional climate models. Glob. Planet. Change, 151, 134-143. https://doi.org/10.1016/j.gloplacha.2016.10.008

Rotunno, R. and Fantini, M. (1989) Petterssen's "Type-B" cyclogenesis in terms of discrete, neutral eady modes. J. Atmos. Sci., 46, 3599-3604. https://doi.org/10.1175/1520-0469(1989)046<3599:PBITOD>2.0.CO;2

Skamarock, W.C., Klemp, J.B., Dudhia, J., Gill, D.O., Liu, Z., Berner, J., Wang, W., Powers, J.G., Duda, M., Barker, D.M. and Huang, X.-Y. (2019) A Description of the Advanced Research WRF Model Version 4. No. NCAR/TN-556+STR. Boulder, CO: NCAR. https://doi.org/10.5065/1dfh-6p97.

Stein, U. and Alpert, P. (1993) Factor separation in numerical simulations. J. Atmos. Res., 50, 2107-2115.

Thompson, G., Field, P.R., Rasmussen, R.M. and Hall, W.D. (2008) Explicit forecasts of winter precipitation using an improved bulk microphysics scheme. Part II: Implementation of a new snow parameterization. Mon. Wea. Rev., 136, 5095–5115. https://doi.org/10.1175/2008MWR2387.1

Toomey, T., Amores, A., Marcos, M., Orfila, A. and Romero, R. (2022) Coastal hazards of tropical-like cyclones over the Mediterranean Sea. J. Geophys. Res. - Oceans, 127, e2021JC017964. https://doi.org/10.1029/2021JC017964.

Trini Castelli, S., Bisignano, A., Donateo, A., Landi, T.C., Martano, P. and Malguzzi, P. (2020) Evaluation of the turbulence parametrization in the MOLOCH meteorological model. Quart. J. Roy. Meteor. Soc., 146, 124–140, https://doi.org/10.1002/qj.3661.

FIGURE CAPTIONS

Figure 1: Selected weather stations in and around the Venice lagoon.

Figure 2: Domains used in the WRF model simulations. The places mentioned in the text are also indicated.

Figure 3: ERA5 reanalysis of 500 hPa geopotential height (colors, in gpdam) and mslp (dark lines, in hPa) at (a) 1200 UTC, 10 November 2019, (b) 0000 UTC and (c) 1200 UTC, 11 November 2019, (d)

0000 UTC, (e) 1200 UTC, and (f) 2100 UTC, November 12, 2019. The red "L" denotes the position of the upper-level low.

Figure 4: Mslp (hPa) between 1700 UTC and 2300 UTC, November 12, 2019 in selected surface stations.

Figure 5: Wind barbs in selected surface stations at six significant time steps during the cyclone transit.

Figure 6: 5-min average wind speed peaks (top) and direction (bottom) recorded in selected weather stations.

Figure 7: Upper panel: Air temperature (T, solid line), dew point temperature (Td, wide dashed line) and relative humidity (RH, narrow dashed line). Bottom panel: sea level pressure. The fields are shown in Piattaforma CNR and Palazzo Cavalli stations.

Figure 8: Mslp at Venice in control runs and observed value (Palazzo Cavalli weather station) – grid 3 (left); cyclone track – grid 1 (right). The tracks in grid 1 are shown since they are smoother than in the inner grid.

Figure 9: Mslp (hPa) and wind speed (m/s) at 1400 UTC, November 12, 2019 (grid 1).

Figure 10: 950 hPa frontogenesis function at 12 UTC (cyan), 15 UTC (blue), 18 UTC (green), 21 UTC (red). The contours refer to 1, 2, 3 $K\,(km)^{-1}h^{-1}$ (the outer the contour, the lower the value). The figure is based on GFS data.

Figure 11: WRF model simulation, Grid 1: 1000 hPa temperature (blue contours; values: 282, 286, 290 K), 700-1000 hPa depth (red contours; values: 2930, 2940, 2950, 2960 gpm), 600-300 hPa depth (green contours; values: 4960, 4980, 5000, 5020, 5040, 5060 gpm), at 14 UTC (top), 18 UTC (middle), 20 UTC (bottom). The isobar of 991.5 hPa is also shown (purple dashed contours) at 18 UTC and 20 UTC to identify the cyclone location.

Figure 12: 950 hPa equivalent potential temperature (K) and wind at 1400 UTC (a), 1800 UTC (b) and 2000 UTC (c), November 12, 2019 (grid 3).

Figure 13: Vertical velocity (colors) and horizontal wind (barbs) at 1900 UTC, November 12, 2019, at 850 hPa (a), 700 hPa (b) and 500 hPa (c) (grid 3).

Figure 14: 300 hPa PV (PVU) at 2000 UTC, November 12, 2019, in run 1112 (a), 1200 (b) and 1212 (c) (grid 1). The bolded “L” denotes the position of the mslp minimum.

Figure 15: Mslp difference (colors; hPa) between the control run and (a) the NoSFFX run, (b) the NoLH run; mslp (colors and contours; hPa) in (c) NoSFFX run, (d) NoLH run, (e) OnlyPBL run, and (f) NoPhys run. Figures are shown at 2130 UTC, November 12, 2019.

Figure 16: (a) Mslp (white contours; hPa) and adiabatic, conserved part of the PV anomaly PVCO (colors; PVU) at 300 hPa; (b) vertical cross section across the cyclone center of equivalent potential temperature (K; colors) and dynamic tropopause (PV = 2 PVU; green line). Figures are shown at 1900 UTC, November 12, 2019, and refer to the NoPhysNoTopo run. The position of the cross section in b) is shown in a).

Figure 17: (a) surface pressure tendency (black line), decomposed into: contributions by 50 hPa geopotential height (DF), integrated column temperature (ITT), evaporation and rainfall (EP), and a residual term (RES). (b) Integrated temperature term (ITT; black line), decomposed into contributions by: horizontal advection (TADV), vertical motion (VMT), and diabatic heating processes due to boundary layer (TBL), microphysics and convection (THD), long-wave (TLW), and short-wave radiation (TSW). Model outputs are reported every 30 minutes, while pressure tendency is shown in $hPa\,h^{-1}$.

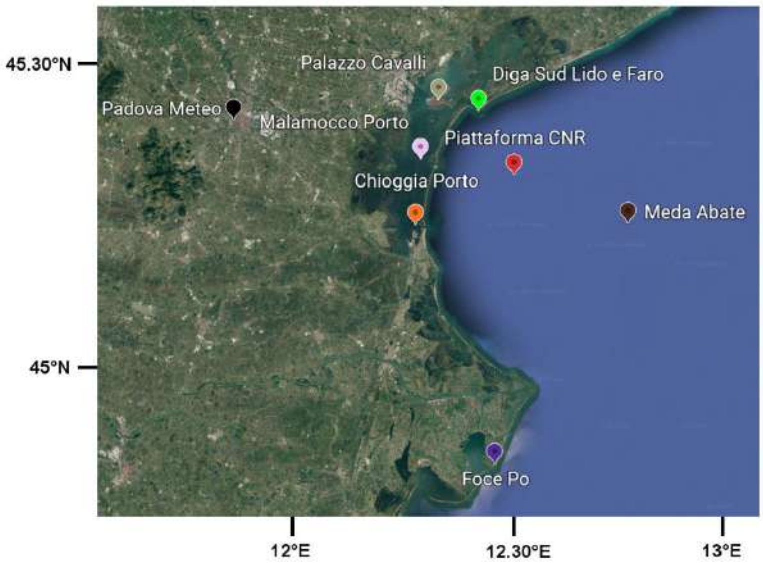

Figure 1: Selected weather stations in and around the Venice lagoon.

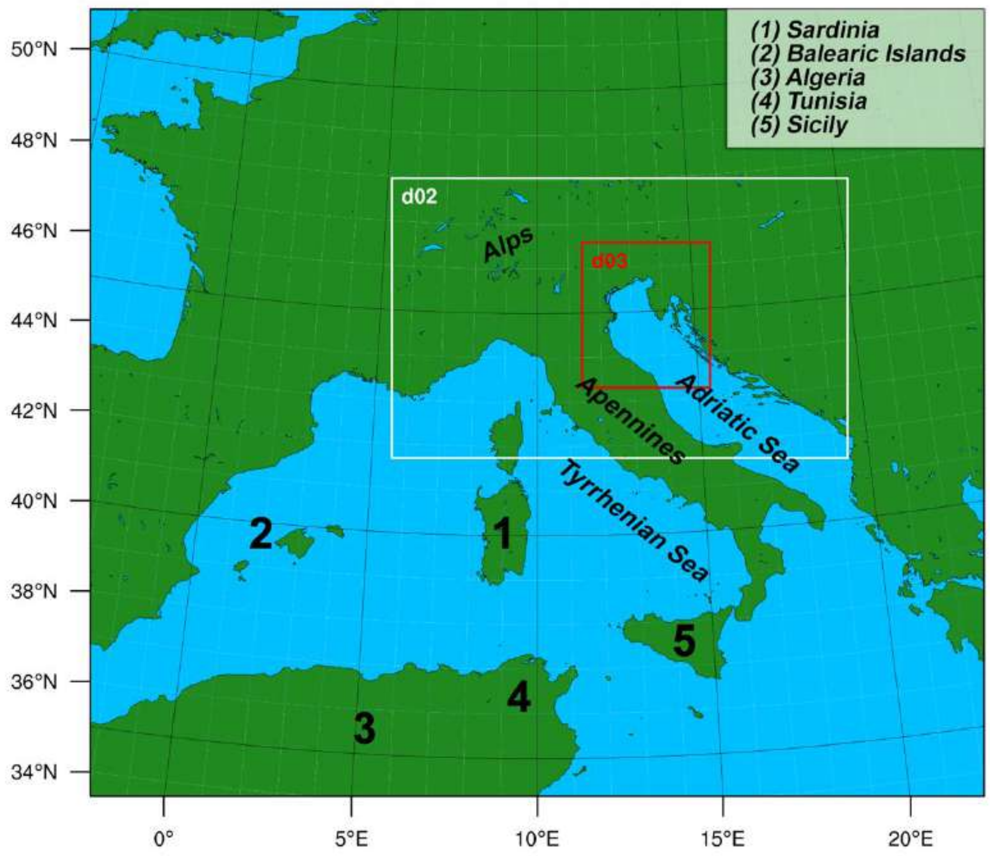

Figure 2: Domains used in the WRF model simulations. The places mentioned in the text are also indicated.

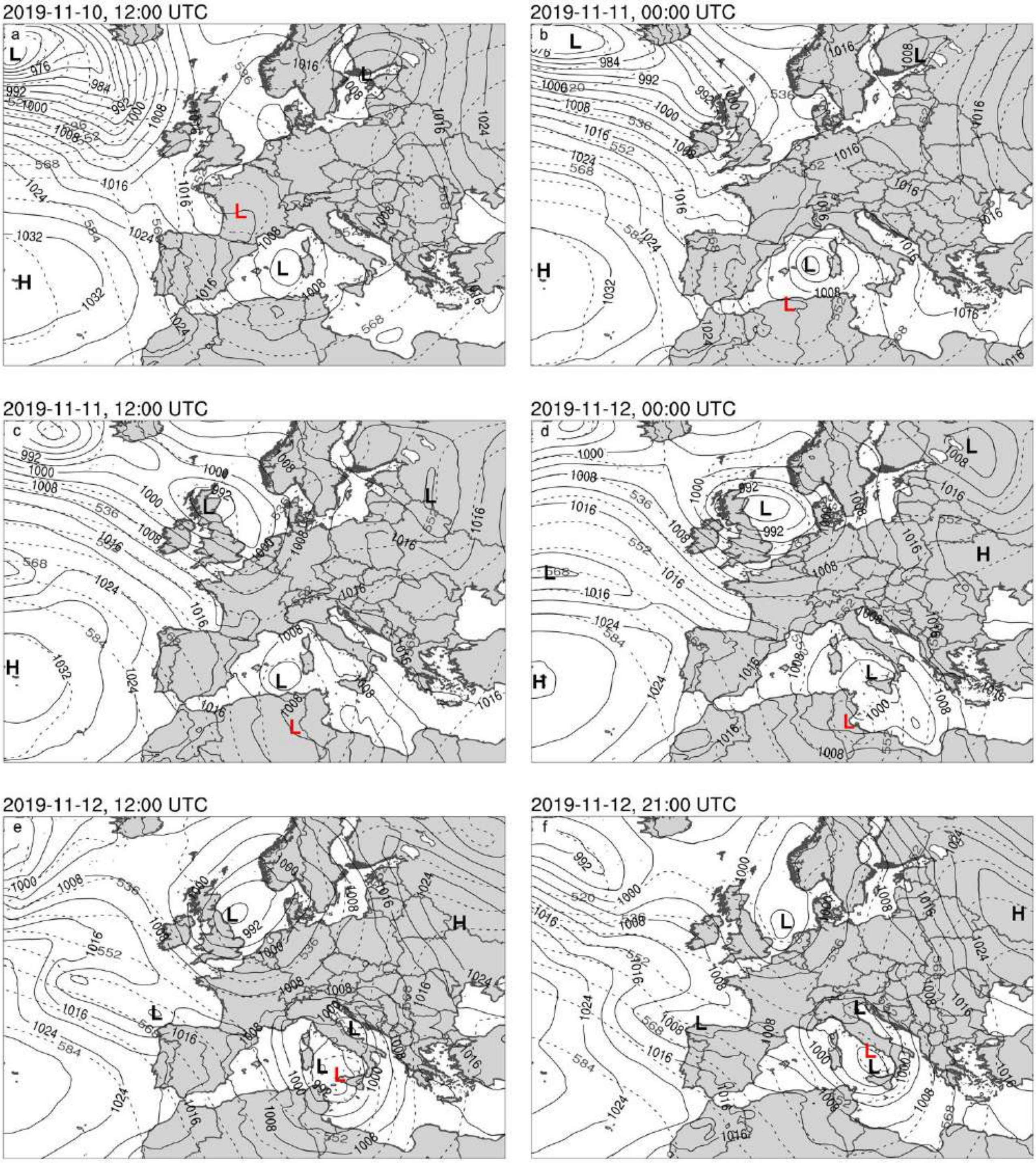

Figure 3: ERA5 reanalysis of 500 hPa geopotential height (colors, in gpdam) and mslp (dark lines, in hPa) at (a) 1200 UTC, 10 November 2019, (b) 0000 UTC and (c) 1200 UTC, 11 November 2019, (d) 0000 UTC, (e) 1200 UTC, and (f) 2100 UTC, November 12, 2019. The red "L" denotes the position of the upper-level low.

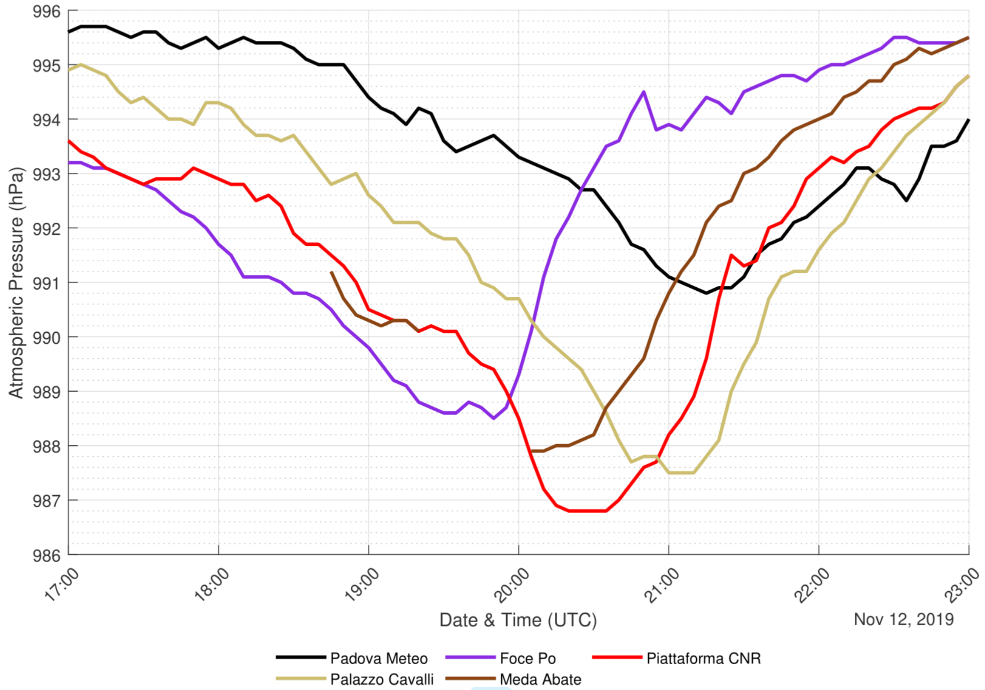

Figure 4: Mslp (hPa) between 1700 UTC and 2300 UTC, November 12, 2019 in selected surface stations.

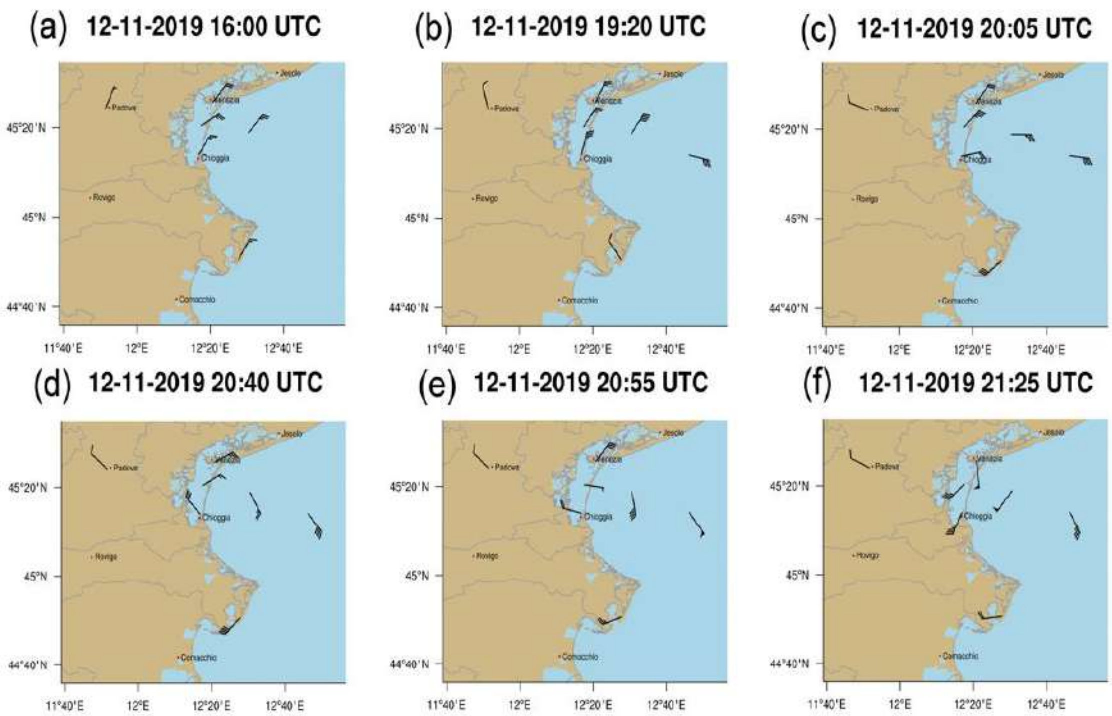

Figure 5: Wind barbs in selected surface stations at six significant time steps during the cyclone transit. Cyclone track estimated from surface observations (bottom right).

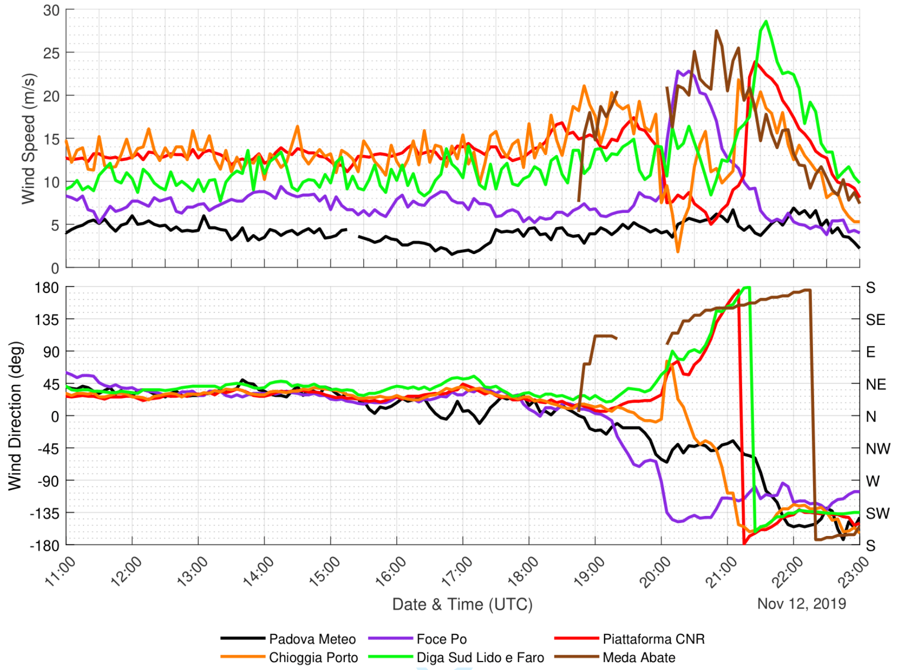

Fig. 6: 5-min average wind speed peaks (top) and direction (bottom) recorded in selected weather stations.

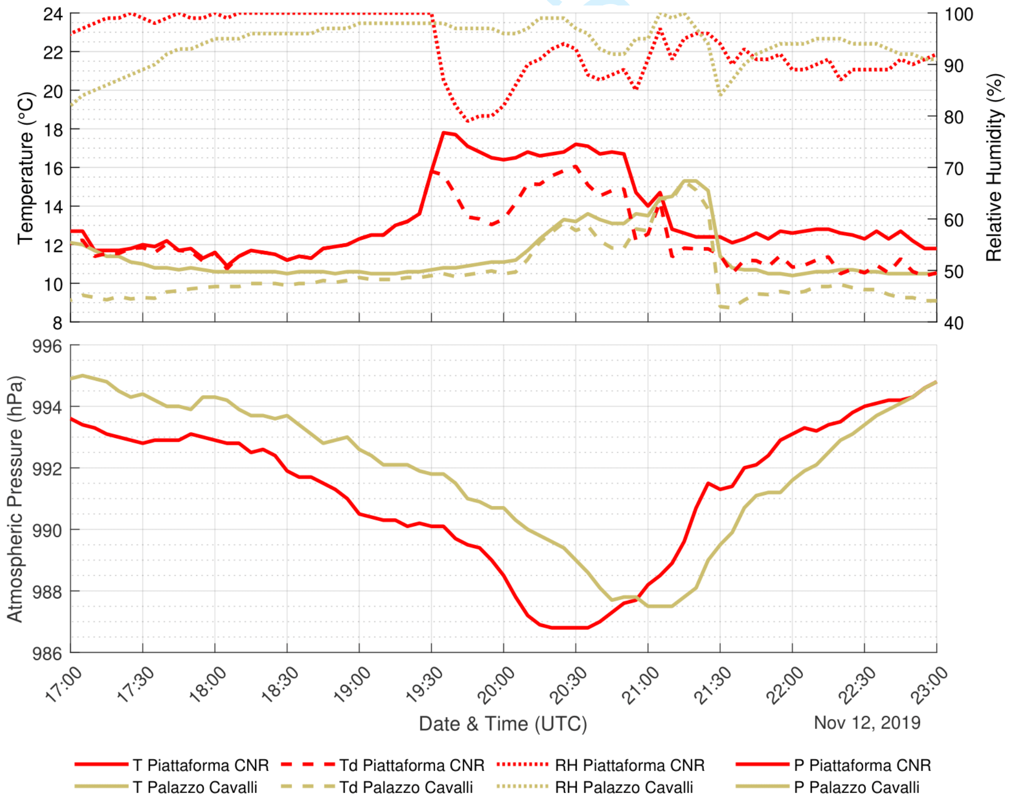

Figure 7: Upper panel: Air temperature (T, solid line), dew point temperature (Td, wide dashed line) and relative humidity (RH, narrow dashed line). Bottom panel: sea level pressure. The fields are shown in Piattaforma CNR and Palazzo Cavalli stations.

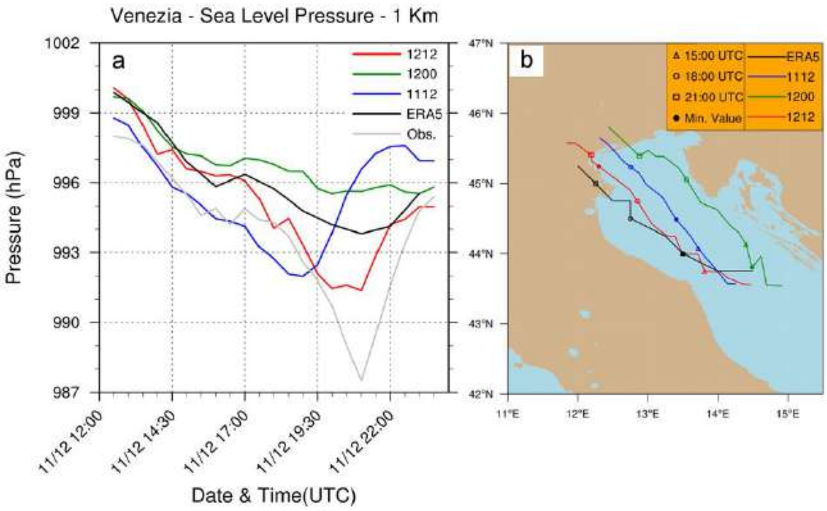

Figure 8: Mslp at Venice in control runs and observed value (Palazzo Cavalli weather station) – grid 3 (left); cyclone track – grid 1 (right). The tracks in grid 1 are shown since they are smoother than in the inner grid.

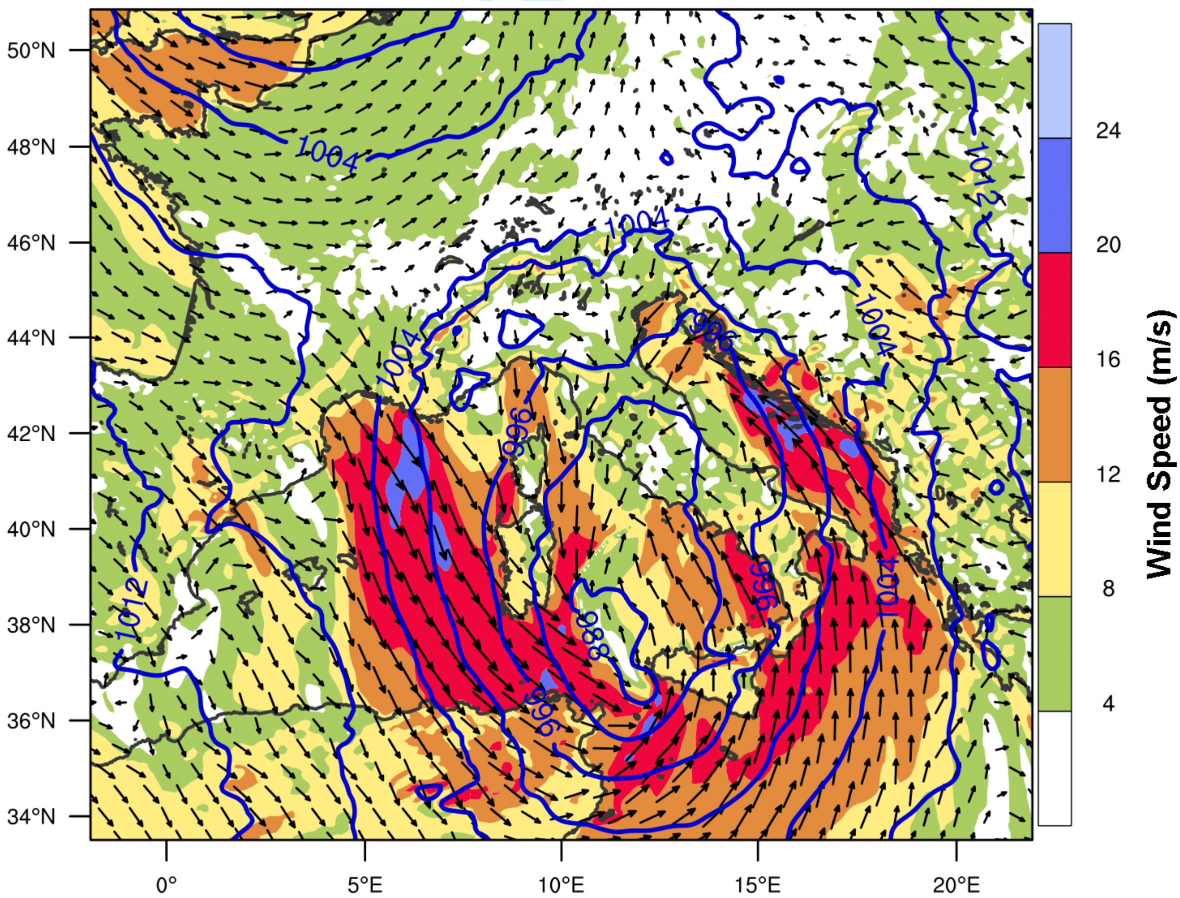

Figure 9: Mslp (hPa) and wind speed (m/s) at 1400 UTC, November 12, 2019 (grid 1).

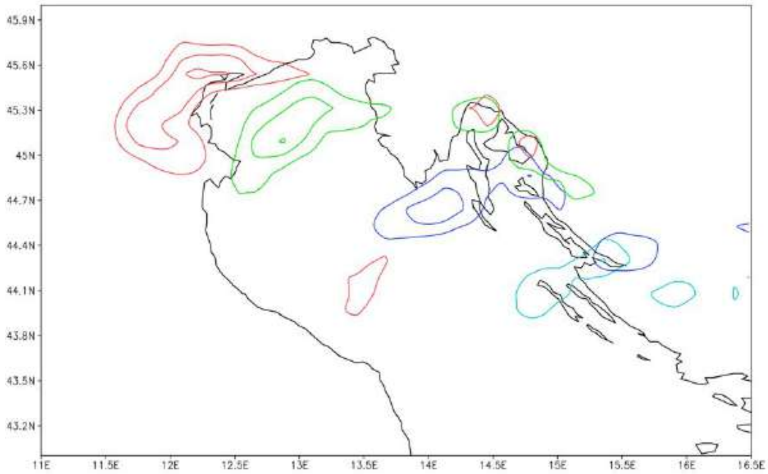

Figure 10: 950 hPa frontogenesis function at 12 UTC (cyan), 15 UTC (blue), 18 UTC (green), 21 UTC (red). The contours refer to 1, 2, 3 $K\,(km)^{-1}h^{-1}$ (the outer the contour, the lower the value). The figure is based on GFS data.

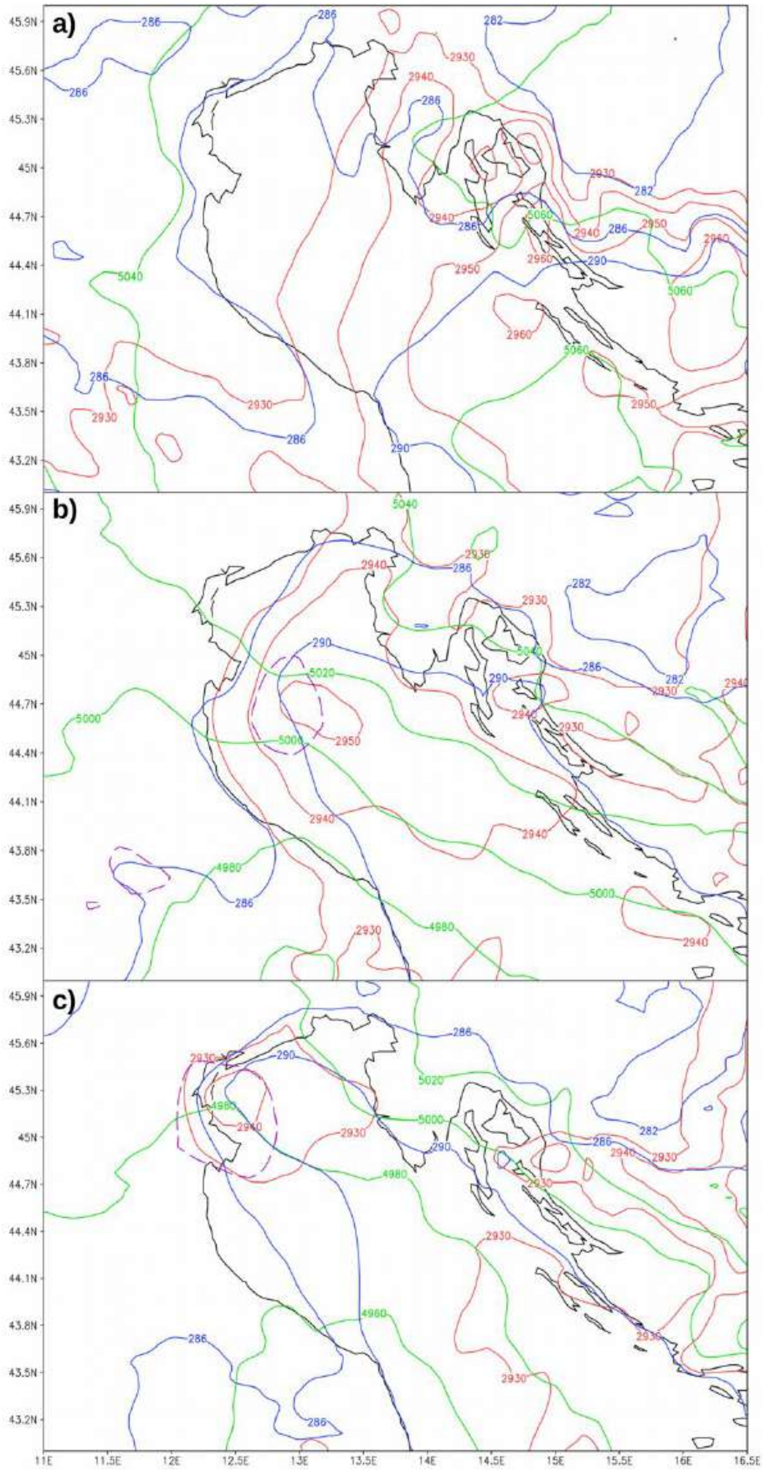

Figure 11: WRF model simulation, Grid 1: 1000 hPa temperature (blue contours; values: 282, 286, 290 K), 700-1000 hPa depth (red contours; values: 2930, 2940, 2950, 2960 gpm), 600-300 hPa depth (green contours; values: 4960, 4980, 5000, 5020, 5040, 5060 gpm), at 14 UTC (top), 18 UTC (middle), 20 UTC (bottom). The isobar of 991.5 hPa is also shown (purple dashed contours) at 18 UTC and 20 UTC to identify the cyclone location.

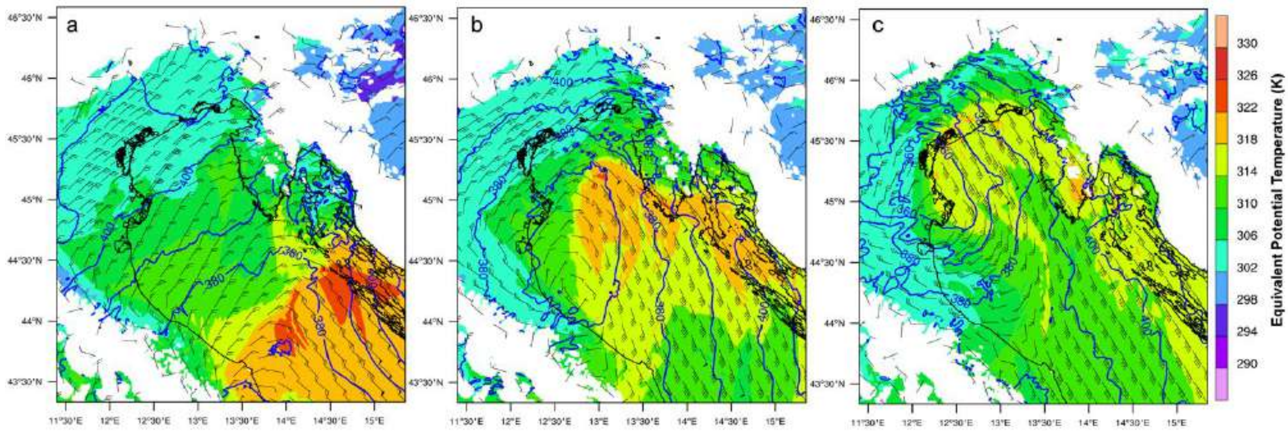

Figure 12: 950 hPa equivalent potential temperature (K) and wind at 1400 UTC (a), 1800 UTC (b) and 2000 UTC (c), November 12, 2019 (grid 3).

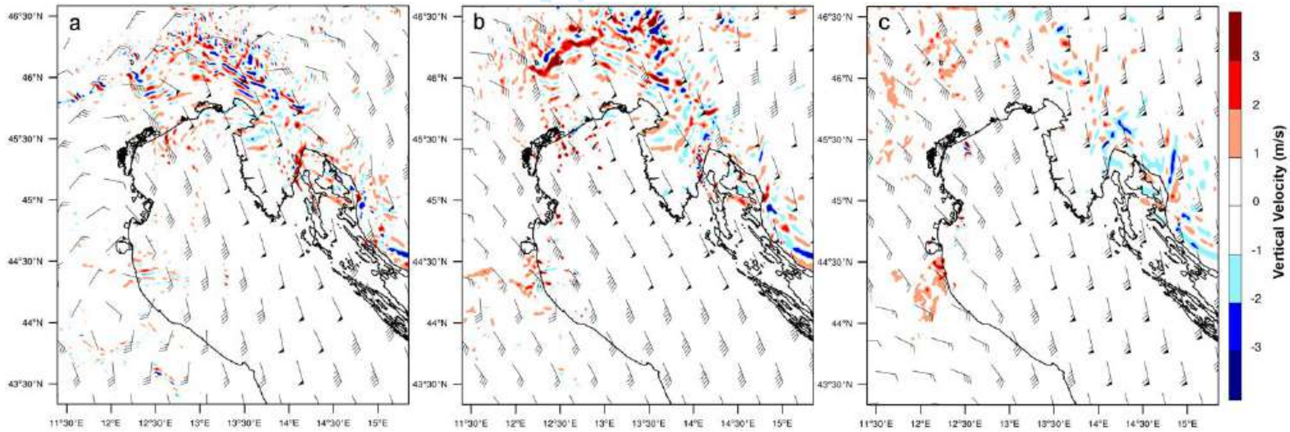

Figure 13: Vertical velocity (colors) and horizontal wind (barbs) at 1900 UTC, November 12, 2019, at 850 hPa (a), 700 hPa (b) and 500 hPa (c) (grid 3).

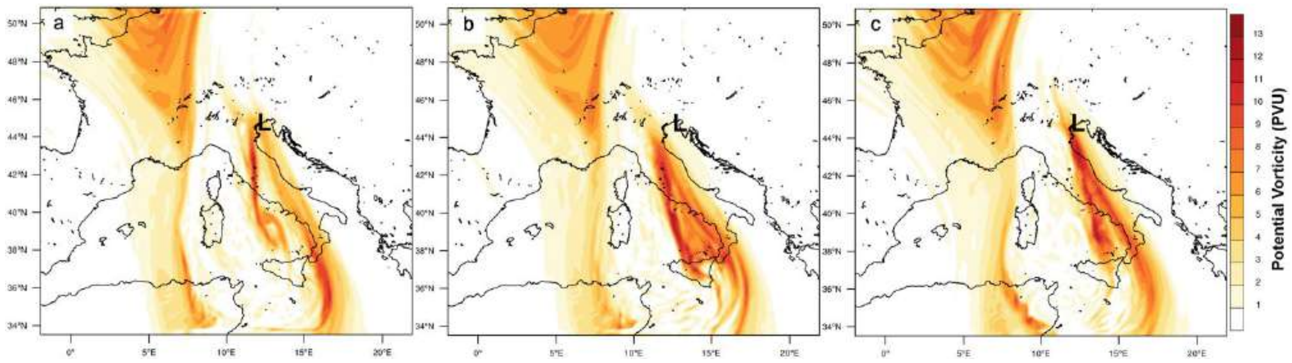

Figure 14: 300 hPa PV (PVU) at 2000 UTC, November 12, 2019, in run 1112 (a), 1200 (b) and 1212 (c) (grid 1). The bolded “L” denotes the position of the mslp minimum.

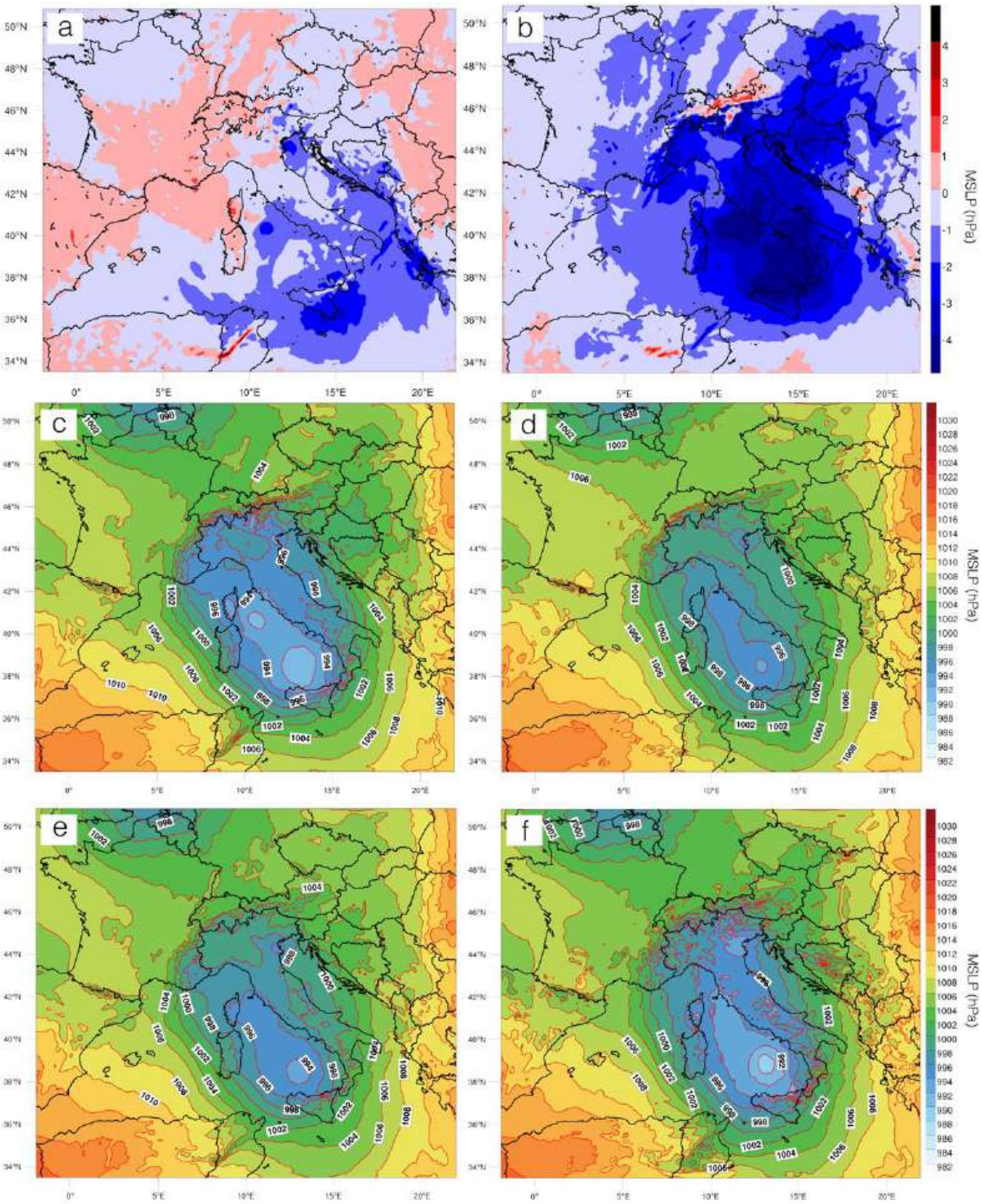

Figure 15: Mslp difference (colors; hPa) between the control run and (a) the NoSFFX run, (b) the NoLH run; mslp (colors and contours; hPa) in (c) NoSFFX run, (d) NoLH run, (e) OnlyPBL run, and (f) NoPhys run. Figures are shown at 2130 UTC, November 12, 2019.

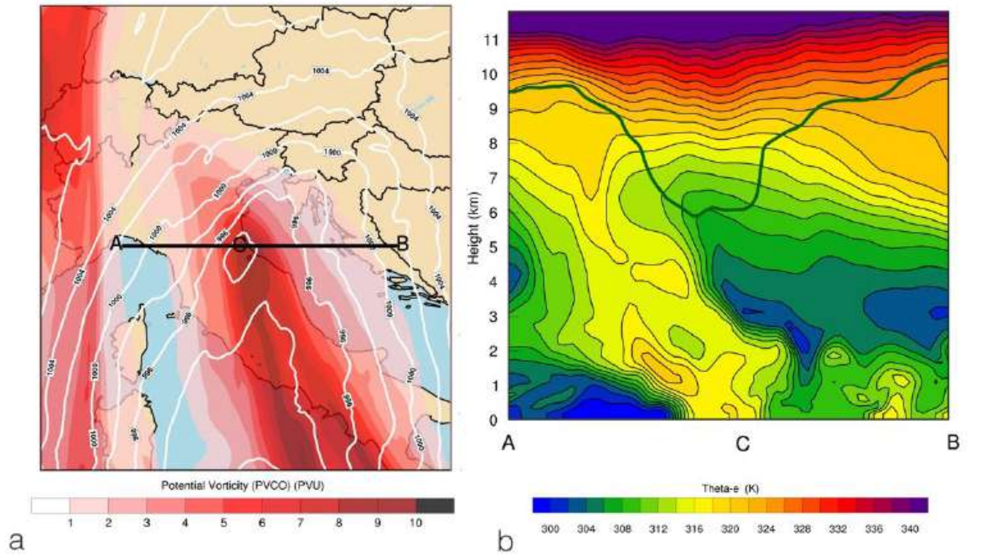

Figure 16: (a) Mslp (white contours; hPa) and adiabatic, conserved part of the PV anomaly PVCO (colors; PVU) at 300 hPa; (b) vertical cross section across the cyclone center of equivalent potential temperature (K; colors) and dynamic tropopause (PV = 2 PVU; green line). Figures are shown at 1900 UTC, November 12, 2019 and refer to the NoPhysNoTopo run. The position of the cross section in b) is shown in a).

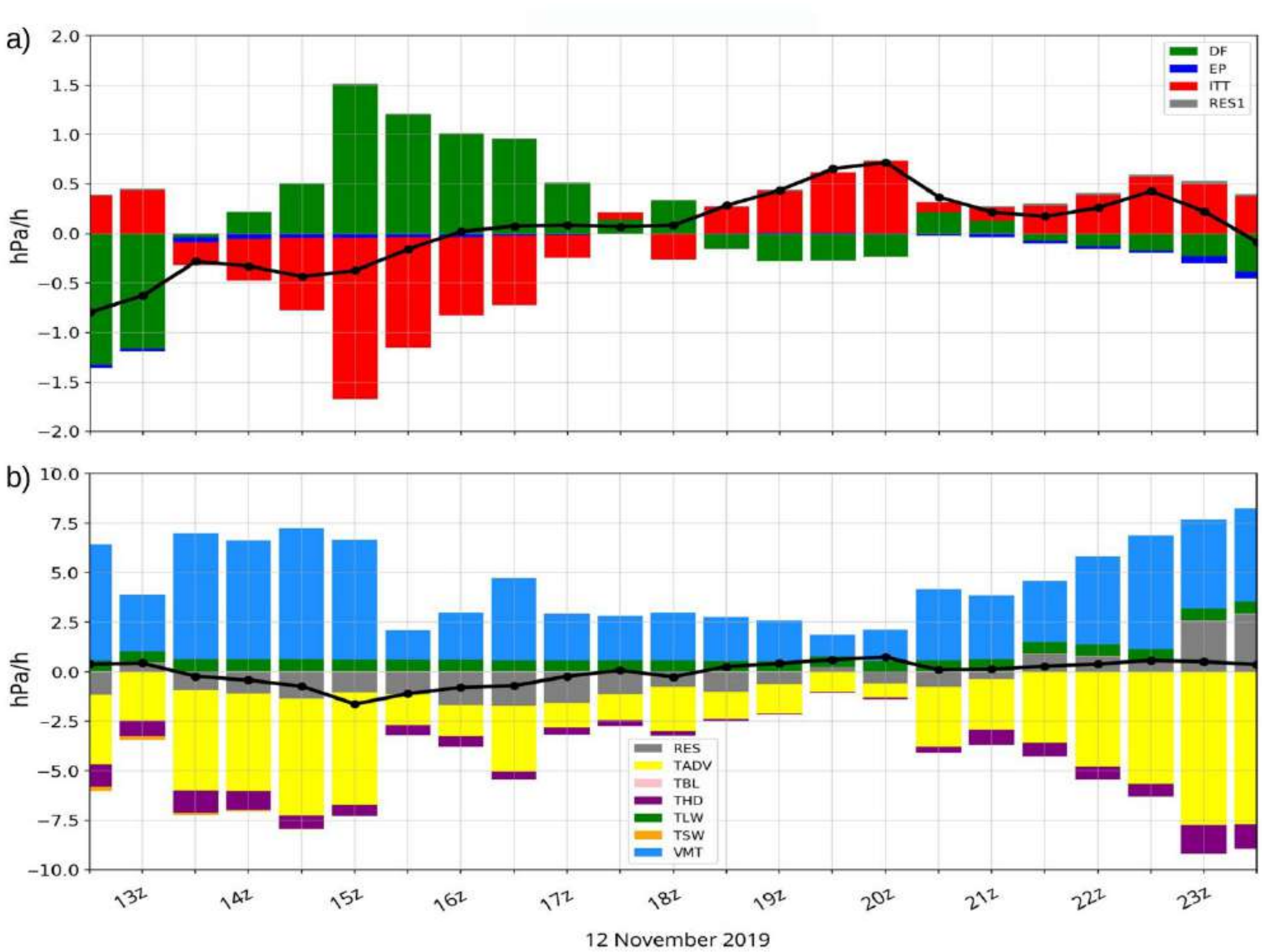

Figure 17: (a) surface pressure tendency (black line), decomposed into: contributions by 50 hPa geopotential height (DF), integrated column temperature (ITT), evaporation and rainfall (EP), and a residual term (RES). (b) Integrated temperature term (ITT; black line), decomposed into contributions by: horizontal advection (TADV), vertical motion (VMT), and diabatic heating processes due to boundary layer (TBL), microphysics and convection (THD), long-wave (TLW), and short-wave radiation (TSW). Model outputs are reported every 30 minutes, while pressure tendency is shown in $hPa\,h^{-1}$.

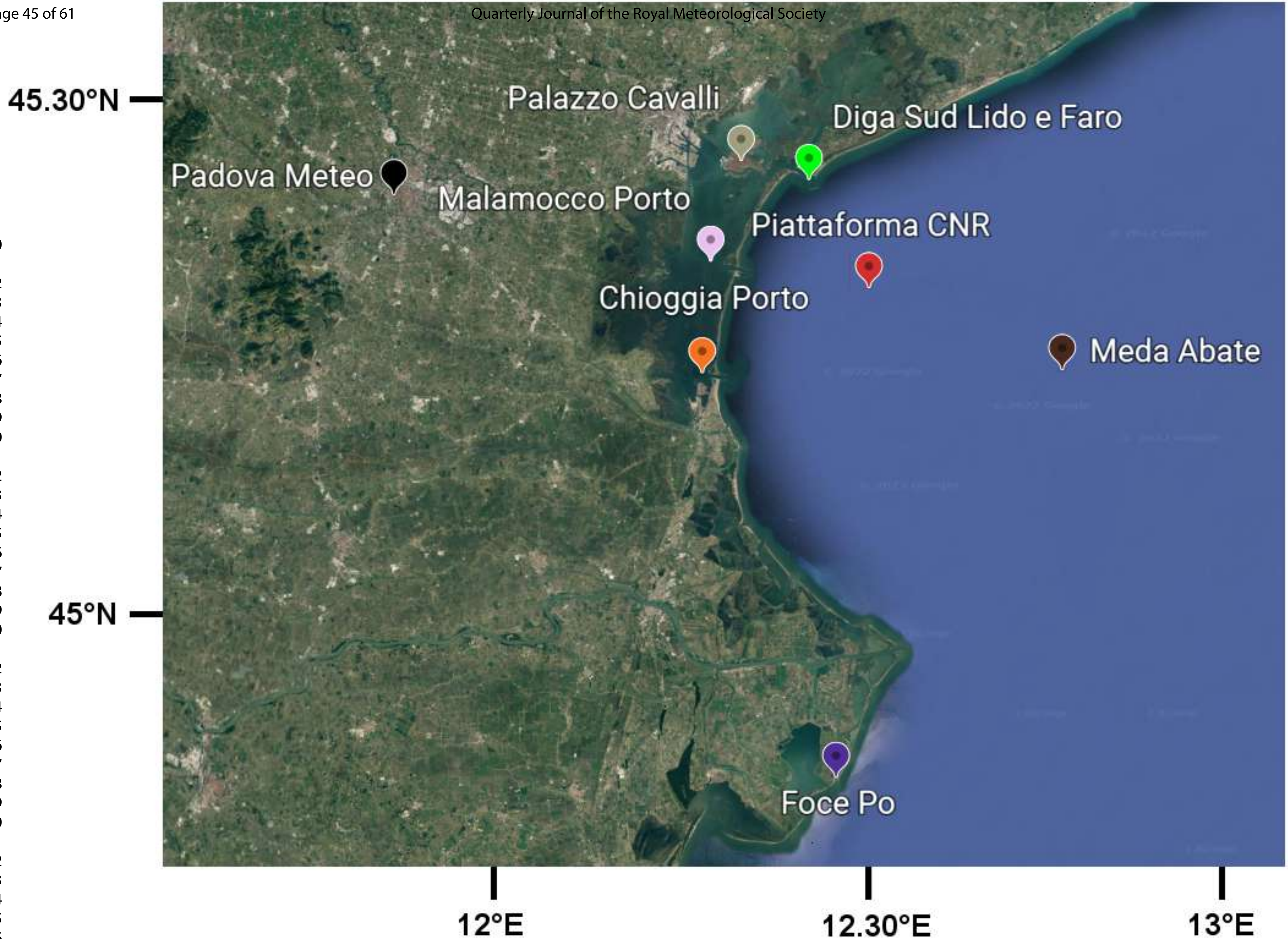
45.30°N
45°N
12°E
12.30°E
13°E
Palazzo Cavalli
Diga Sud Lido e Faro
Padova Meteo
Malamocco Porto
Piattaforma CNR
Chioggia Porto
Meda Abate
Foce Po

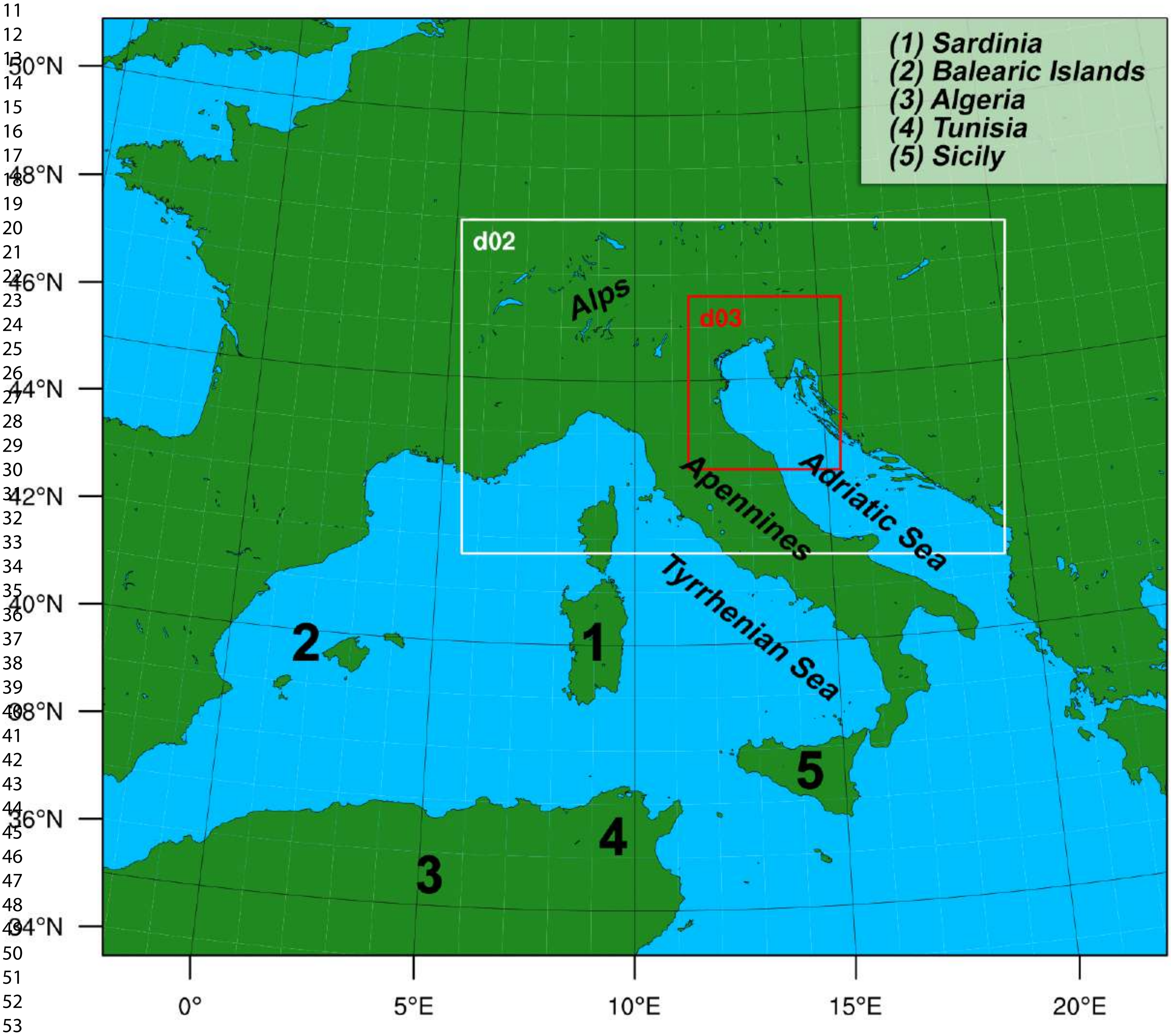

(1) Sardinia
(2) Balearic Islands
(3) Algeria
(4) Tunisia
(5) Sicily
d02
d03
Alps
Apennines
Adriatic Sea
Tyrrhenian Sea
1
2
3
4
5
50°N
48°N
46°N
44°N
42°N
40°N
38°N
36°N
34°N
0°
5°E
10°E
15°E
20°E

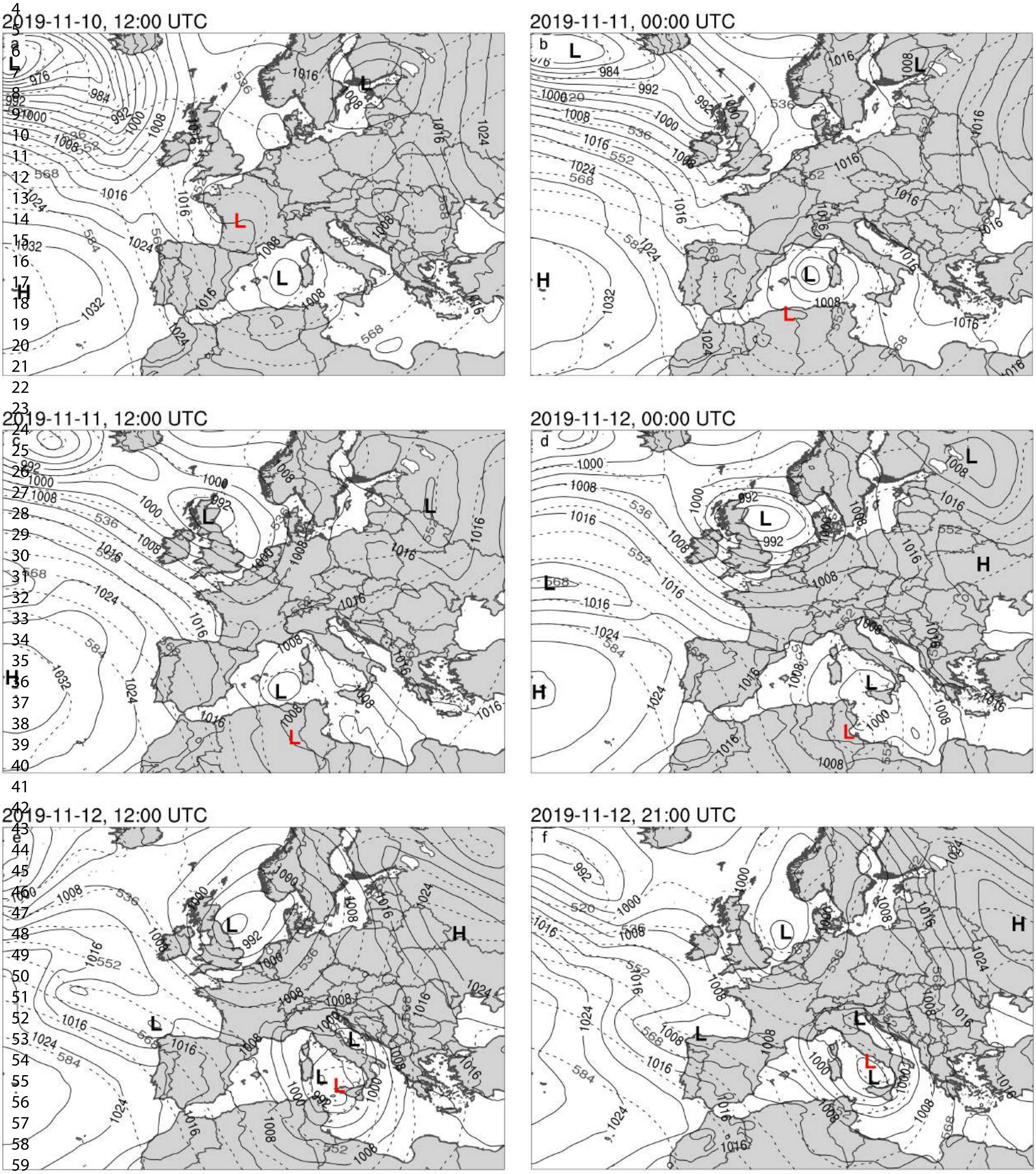
2019-11-10, 12:00 UTC
a
2019-11-11, 00:00 UTC
b
2019-11-11, 12:00 UTC
c
2019-11-12, 00:00 UTC
d
2019-11-12, 12:00 UTC
e
2019-11-12, 21:00 UTC
f

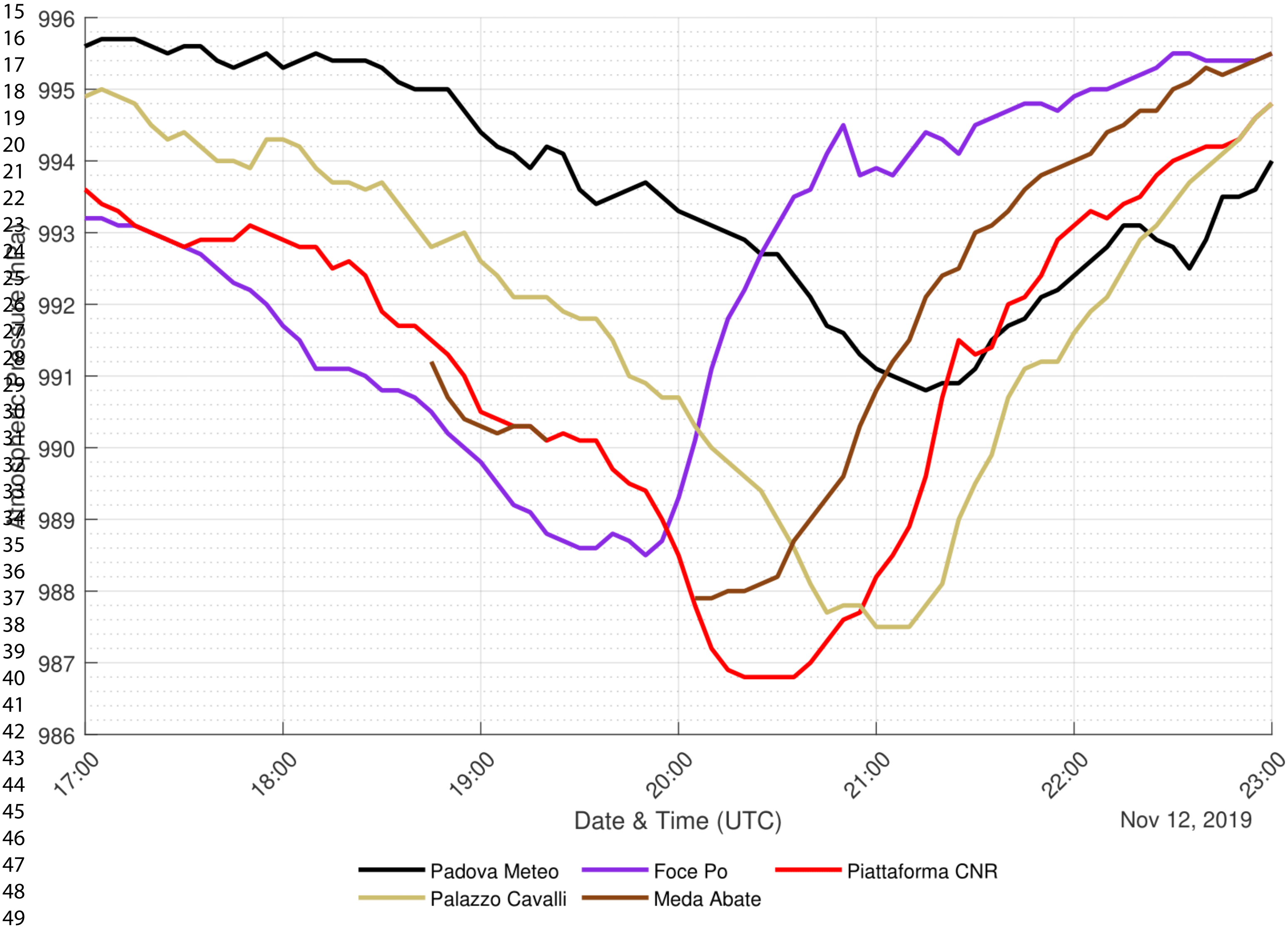
996
995
994
993
992
991
990
989
988
987
986
17:00
18:00
19:00
20:00
21:00
22:00
23:00
Date & Time (UTC)
Nov 12, 2019
Padova Meteo
Foce Po
Piattaforma CNR
Palazzo Cavalli
Meda Abate

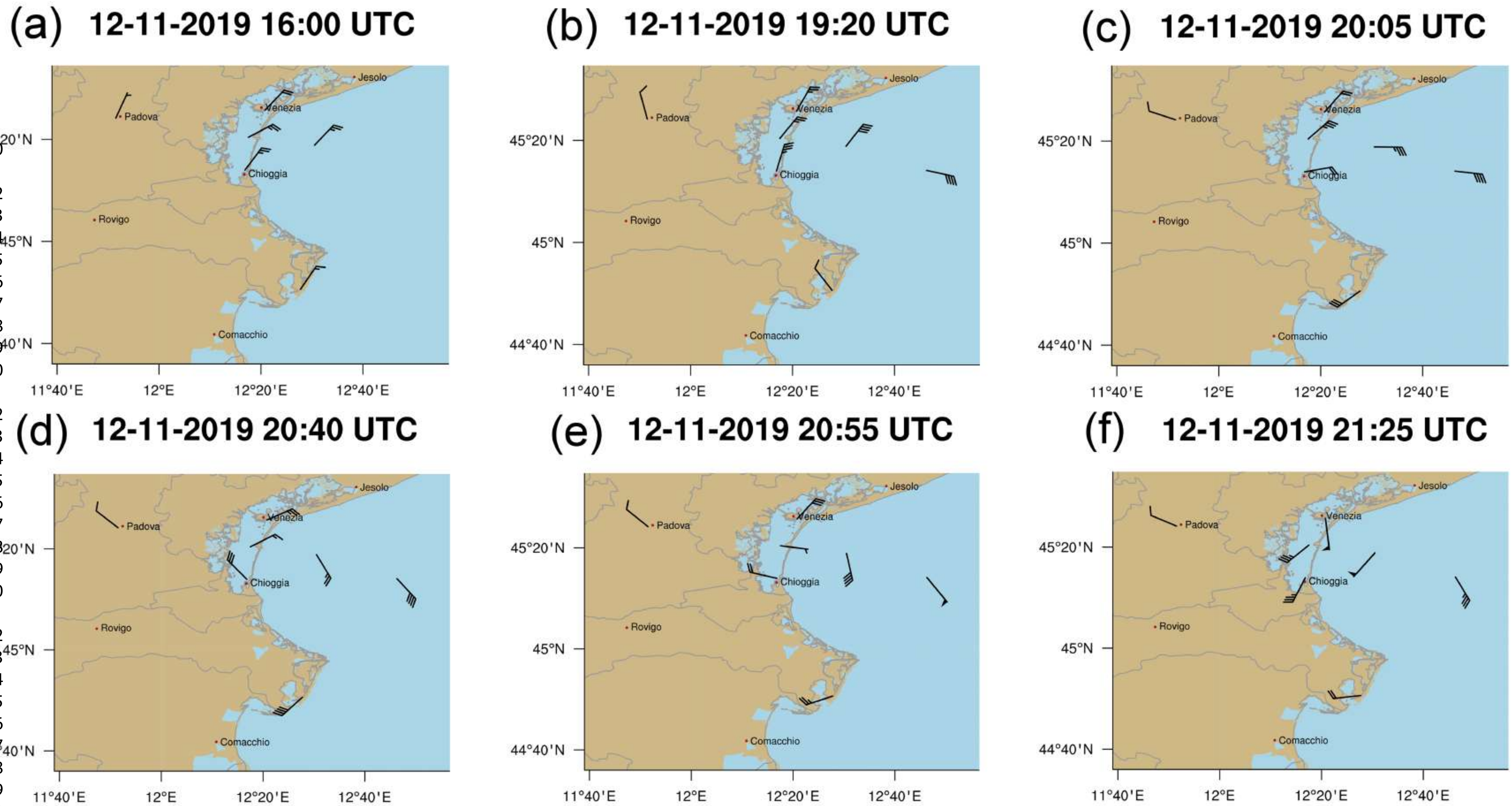
(a) 12-11-2019 16:00 UTC
(b) 12-11-2019 19:20 UTC
(c) 12-11-2019 20:05 UTC
(d) 12-11-2019 20:40 UTC
(e) 12-11-2019 20:55 UTC
(f) 12-11-2019 21:25 UTC
Jesolo
Venezia
Padova
Chioggia
Rovigo
Comacchio
45°20'N
45°N
44°40'N
11°40'E
12°E
12°20'E
12°40'E

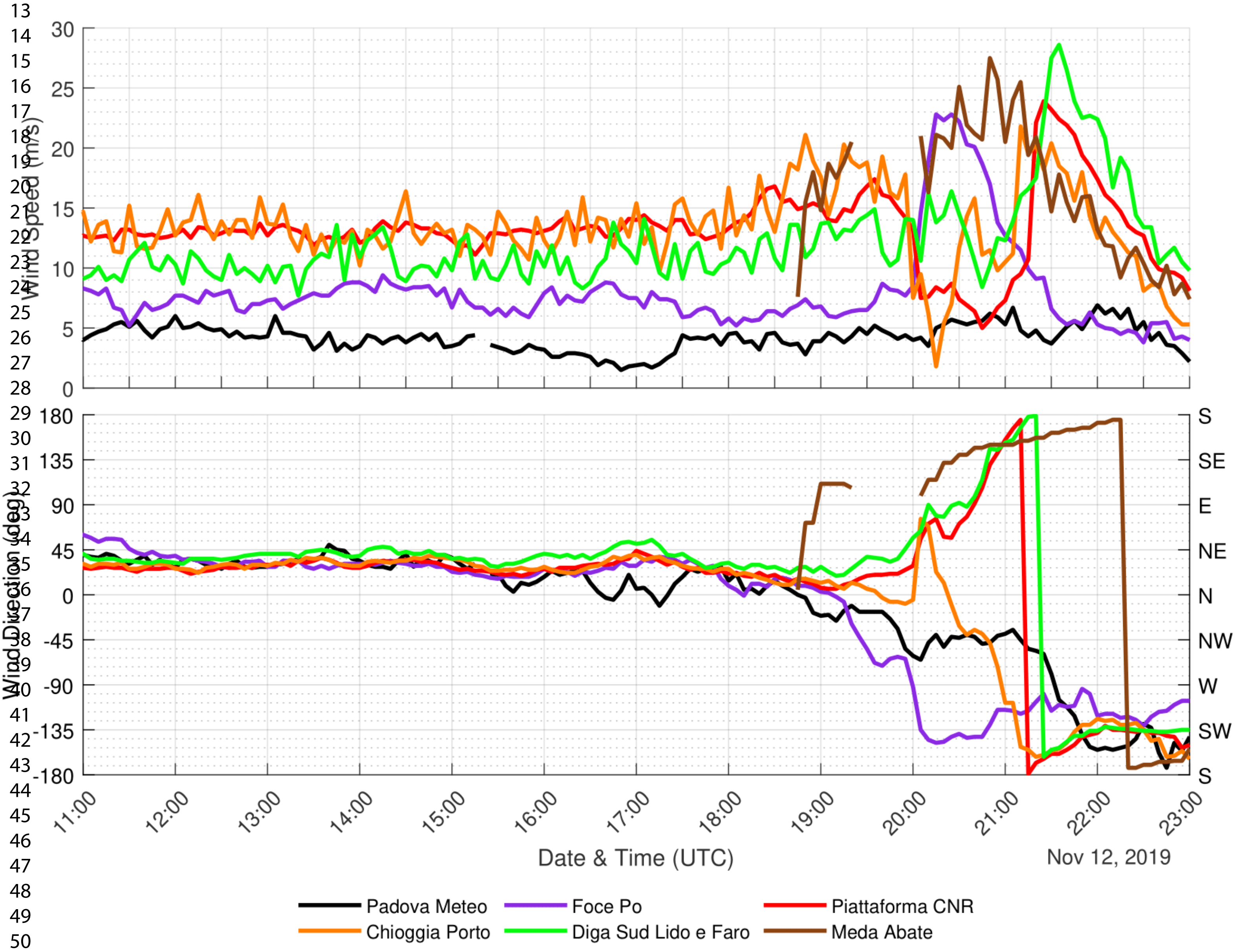
Wind Speed (m/s)
Wind Direction (deg)
S
SE
E
NE
N
NW
W
SW
S
11:00
12:00
13:00
14:00
15:00
16:00
17:00
18:00
19:00
20:00
21:00
22:00
23:00
Date & Time (UTC)
Nov 12, 2019
Padova Meteo
Foce Po
Piattaforma CNR
Chioggia Porto
Diga Sud Lido e Faro
Meda Abate

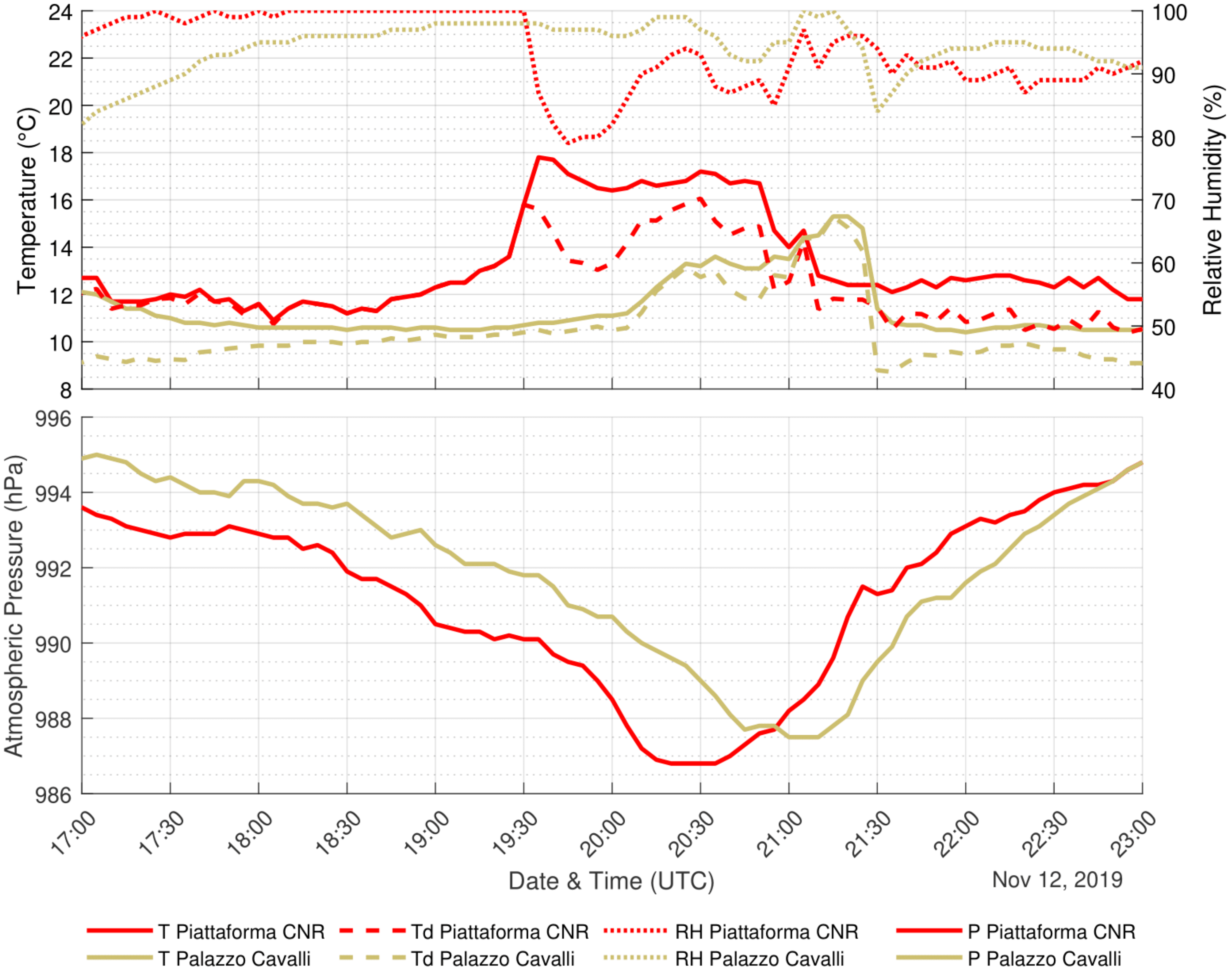
Temperature (°C)
Relative Humidity (%)
Atmospheric Pressure (hPa)
Date & Time (UTC)
Nov 12, 2019
17:00
17:30
18:00
18:30
19:00
19:30
20:00
20:30
21:00
21:30
22:00
22:30
23:00
T Piattaforma CNR
Td Piattaforma CNR
RH Piattaforma CNR
P Piattaforma CNR
T Palazzo Cavalli
Td Palazzo Cavalli
RH Palazzo Cavalli
P Palazzo Cavalli

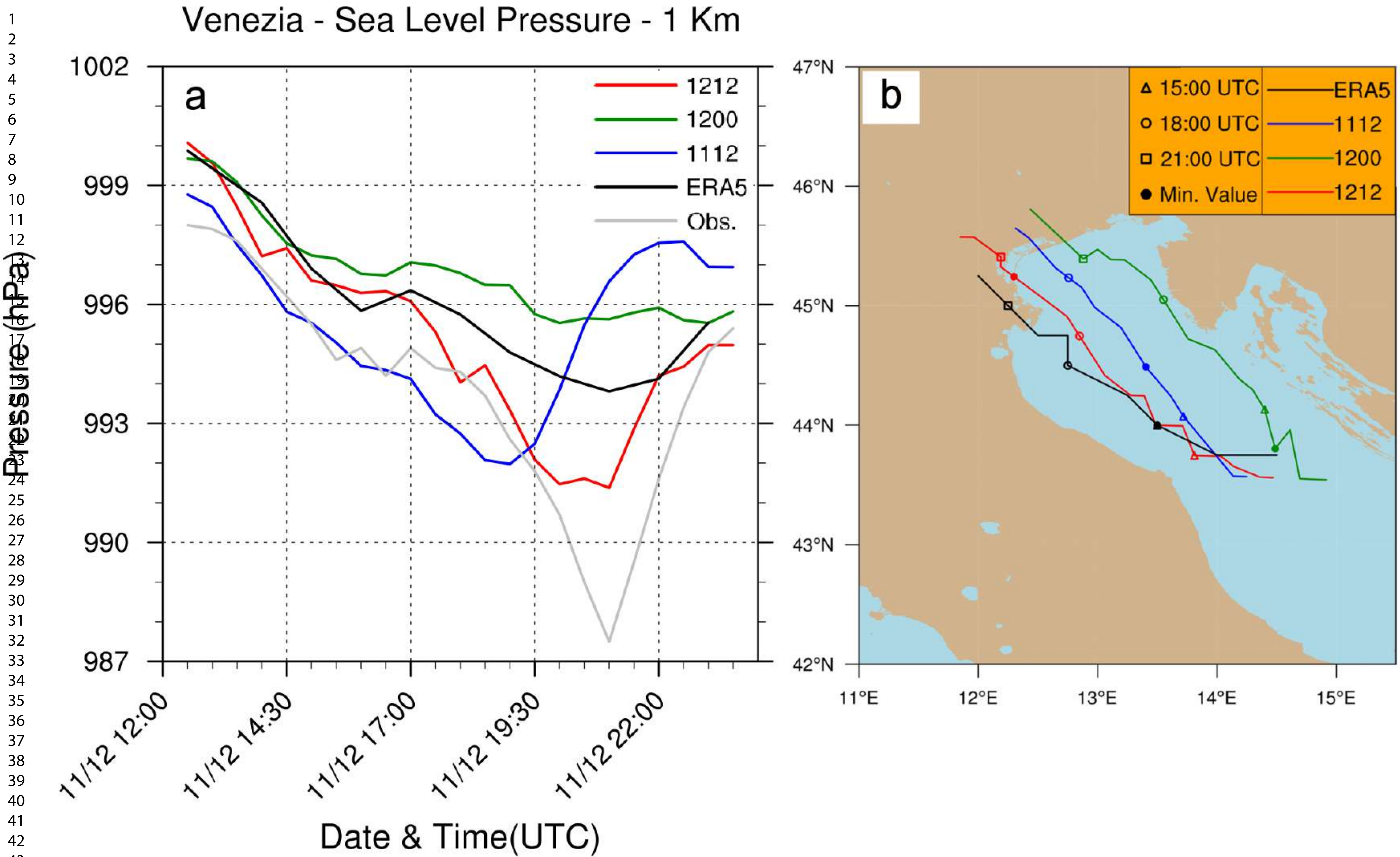
Venezia - Sea Level Pressure - 1 Km
a
1212
1200
1112
ERA5
Obs.
Pressure (hPa)
1002
999
996
993
990
987
11/12 12:00
11/12 14:30
11/12 17:00
11/12 19:30
11/12 22:00
Date & Time(UTC)
b
15:00 UTC
18:00 UTC
21:00 UTC
Min. Value
ERA5
1112
1200
1212
47°N
46°N
45°N
44°N
43°N
42°N
11°E
12°E
13°E
14°E
15°E

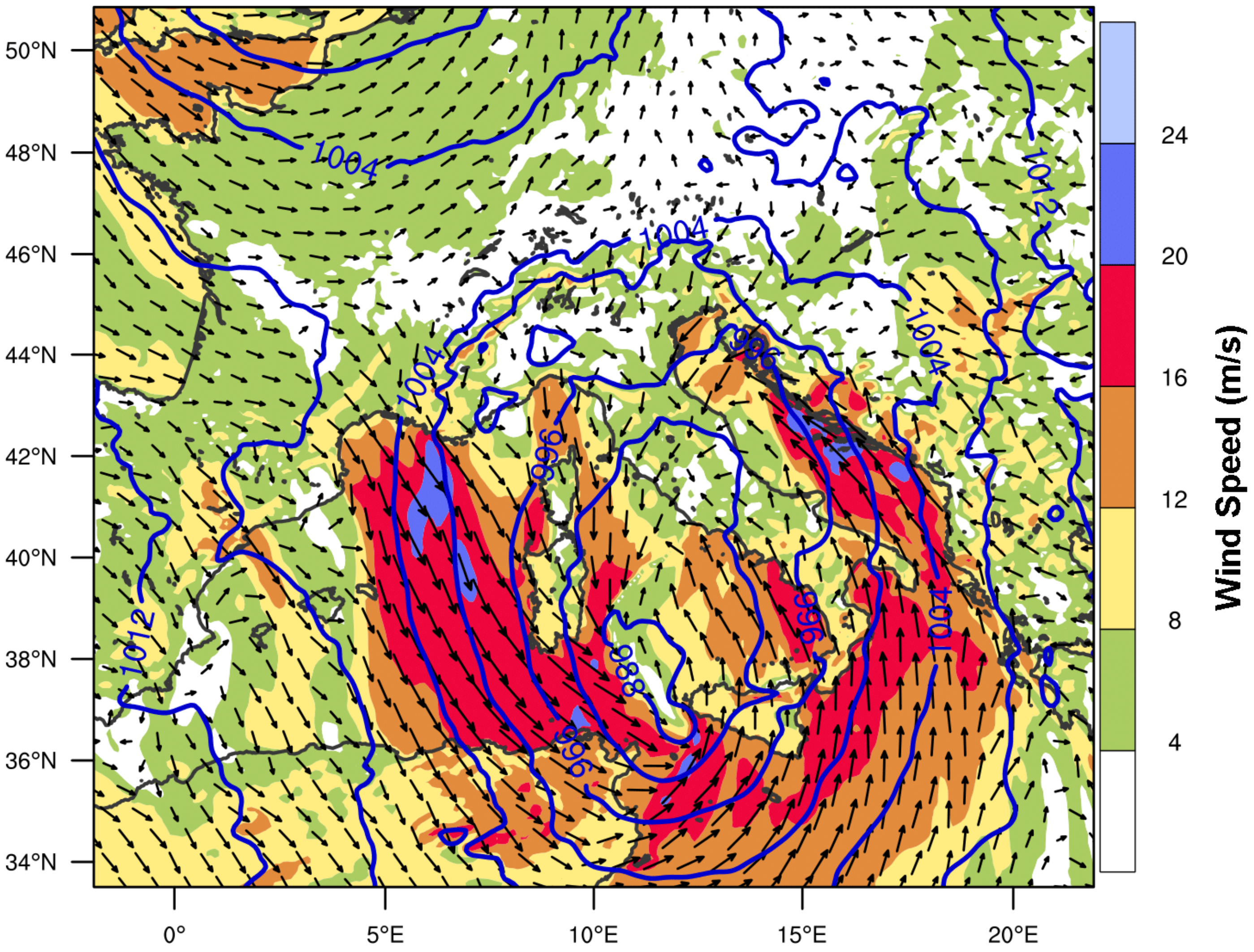
1004
1004
1004
1004
1012
1012
996
996
996
996
988
1004
50°N
48°N
46°N
44°N
42°N
40°N
38°N
36°N
34°N
0°
5°E
10°E
15°E
20°E
4
8
12
16
20
24
Wind Speed (m/s)

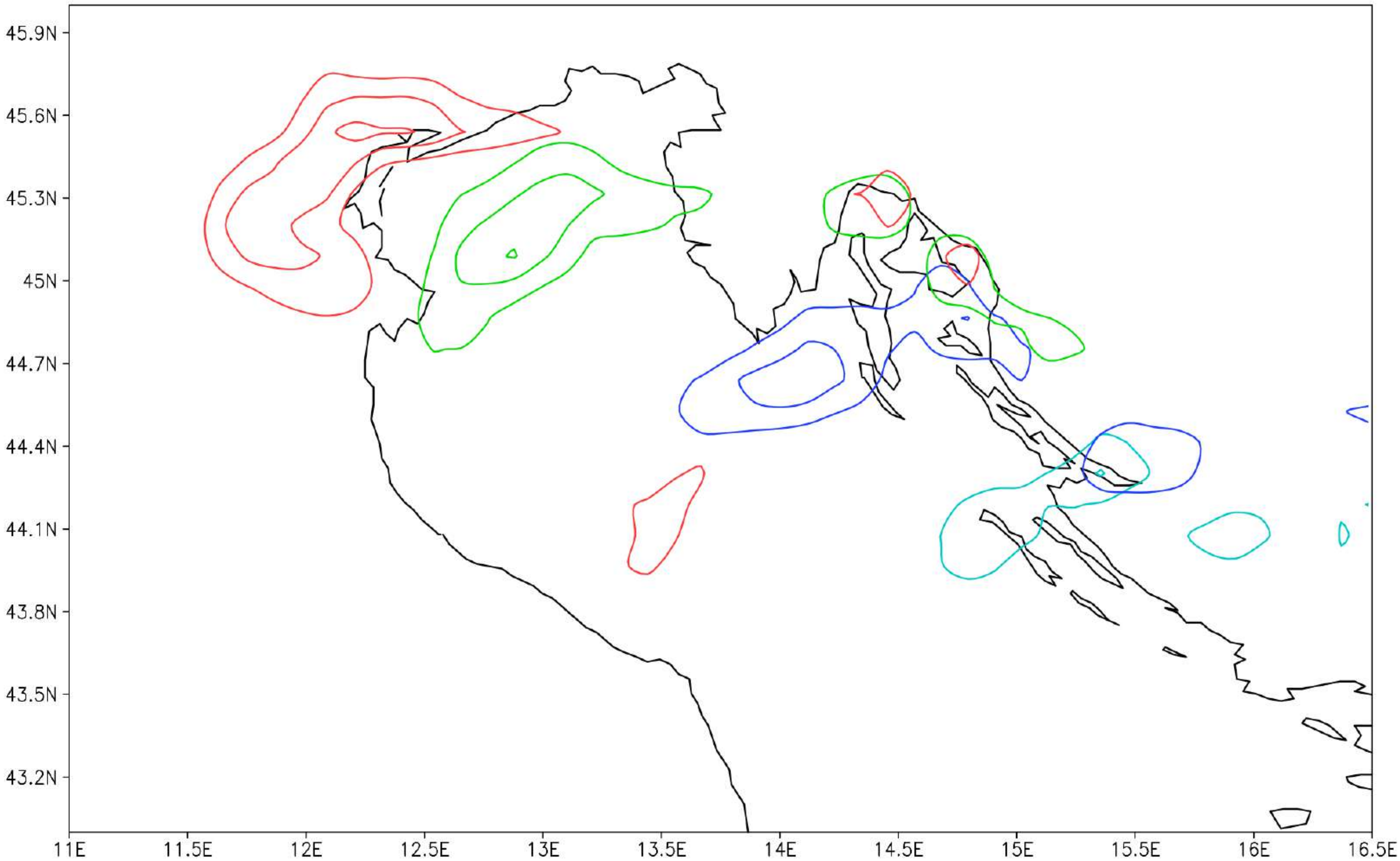
45.9N
45.6N
45.3N
45N
44.7N
44.4N
44.1N
43.8N
43.5N
43.2N
11E
11.5E
12E
12.5E
13E
13.5E
14E
14.5E
15E
15.5E
16E
16.5E

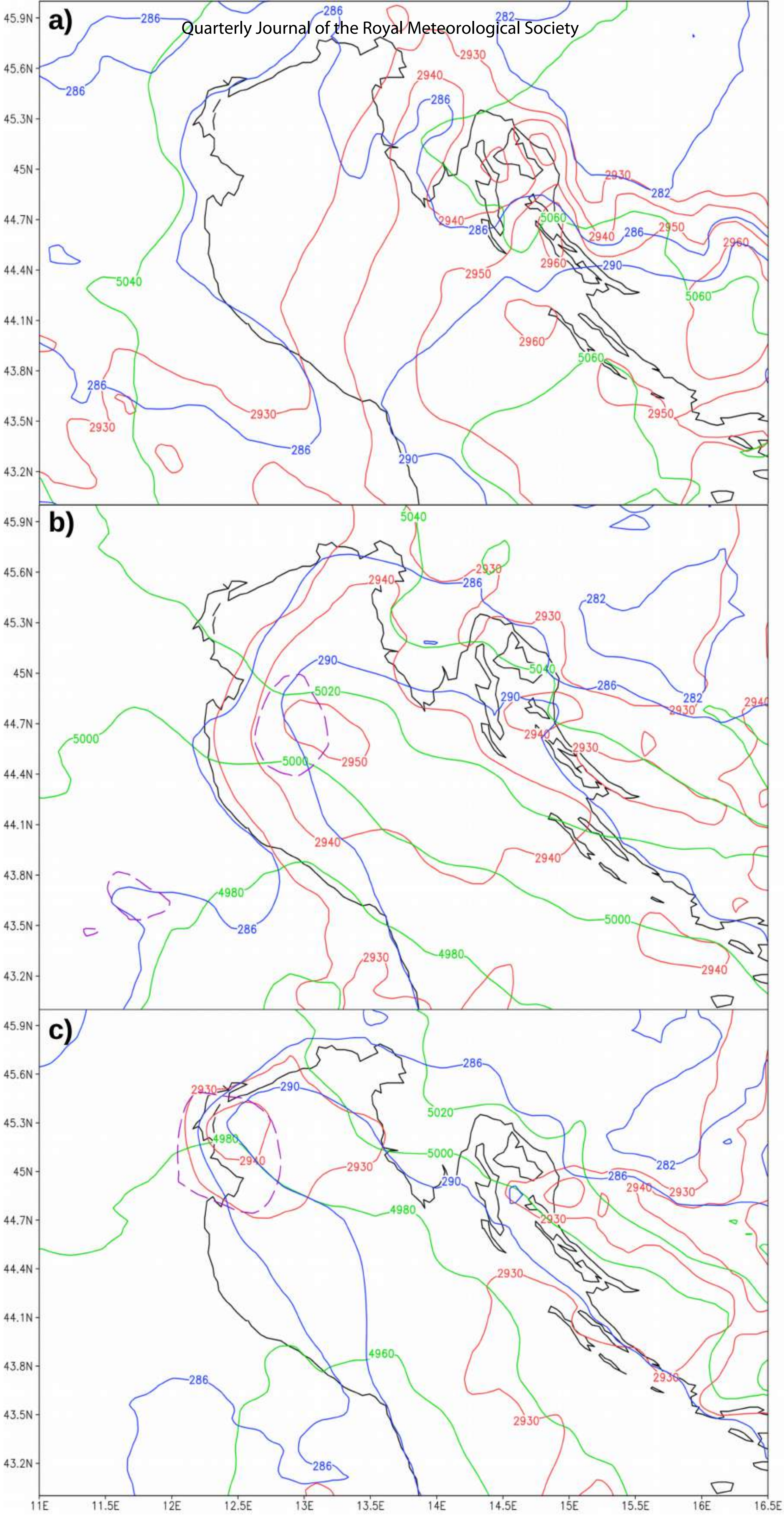
a)
b)
c)
45.9N
45.6N
45.3N
45N
44.7N
44.4N
44.1N
43.8N
43.5N
43.2N
11E
11.5E
12E
12.5E
13E
13.5E
14E
14.5E
15E
15.5E
16E
16.5E
286
282
290
2930
2940
2950
2960
5040
5060
5020
5000
4980
4960

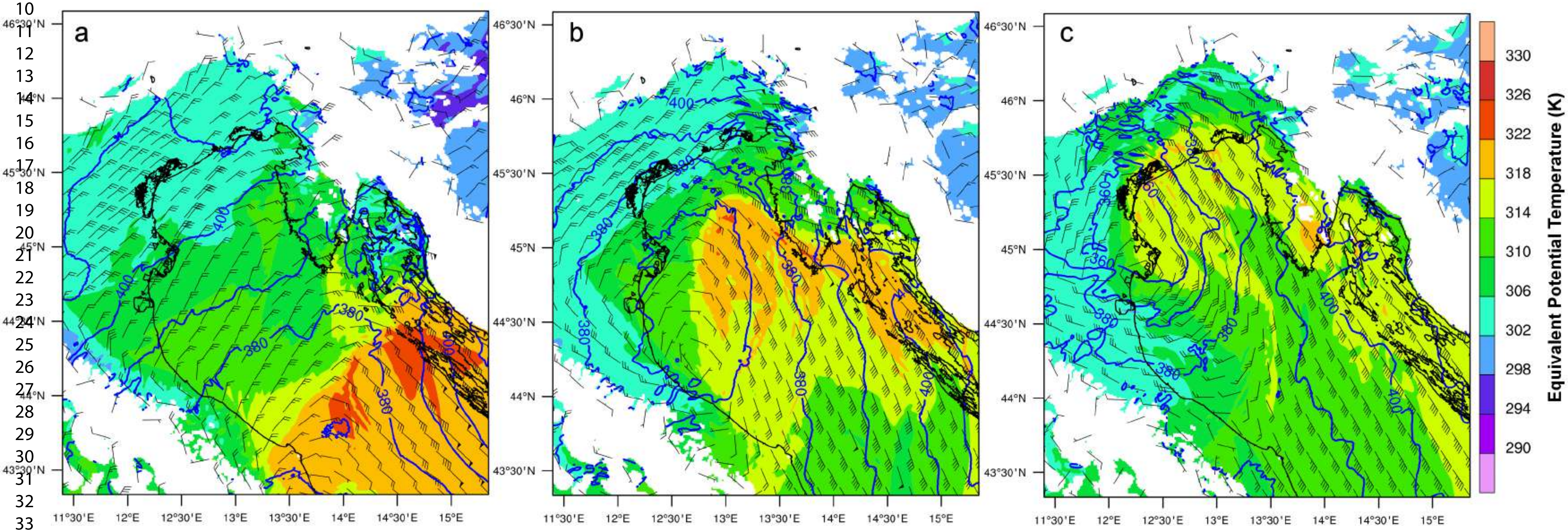
a
b
c
46°30'N
46°N
45°30'N
45°N
44°30'N
44°N
43°30'N
11°30'E
12°E
12°30'E
13°E
13°30'E
14°E
14°30'E
15°E
400
380
360
Equivalent Potential Temperature (K)
330
326
322
318
314
310
306
302
298
294
290

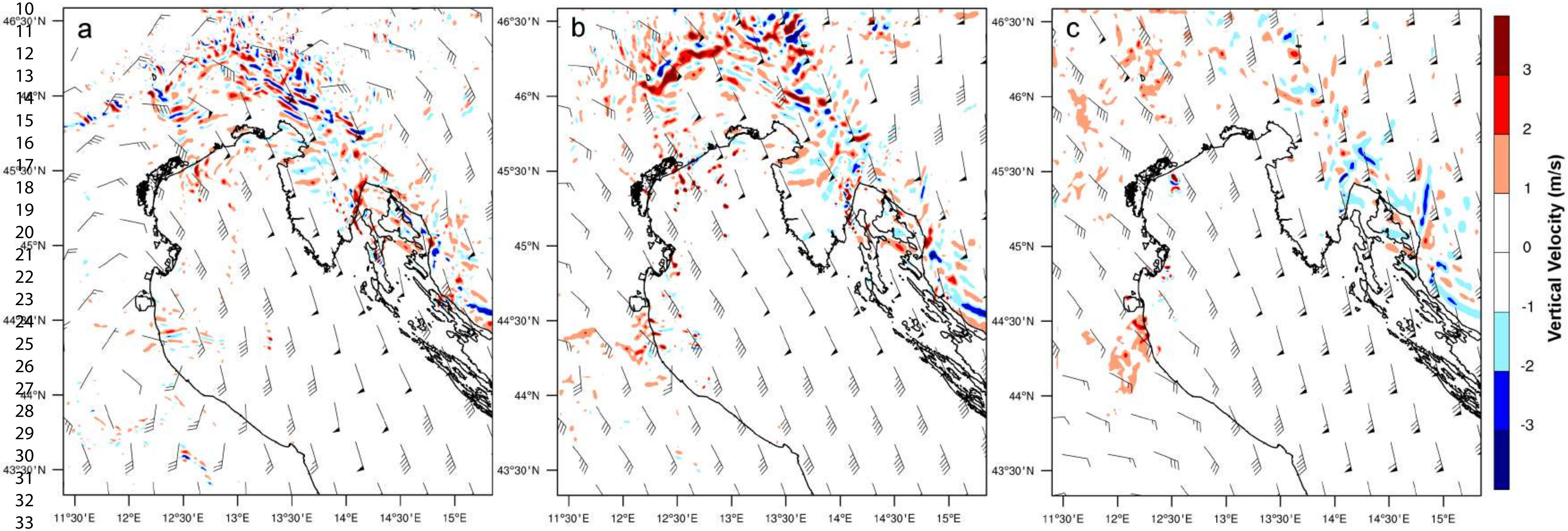
a
b
c
46°30'N
46°N
45°30'N
45°N
44°30'N
44°N
43°30'N
11°30'E
12°E
12°30'E
13°E
13°30'E
14°E
14°30'E
15°E
Vertical Velocity (m/s)
3
2
1
0
-1
-2
-3

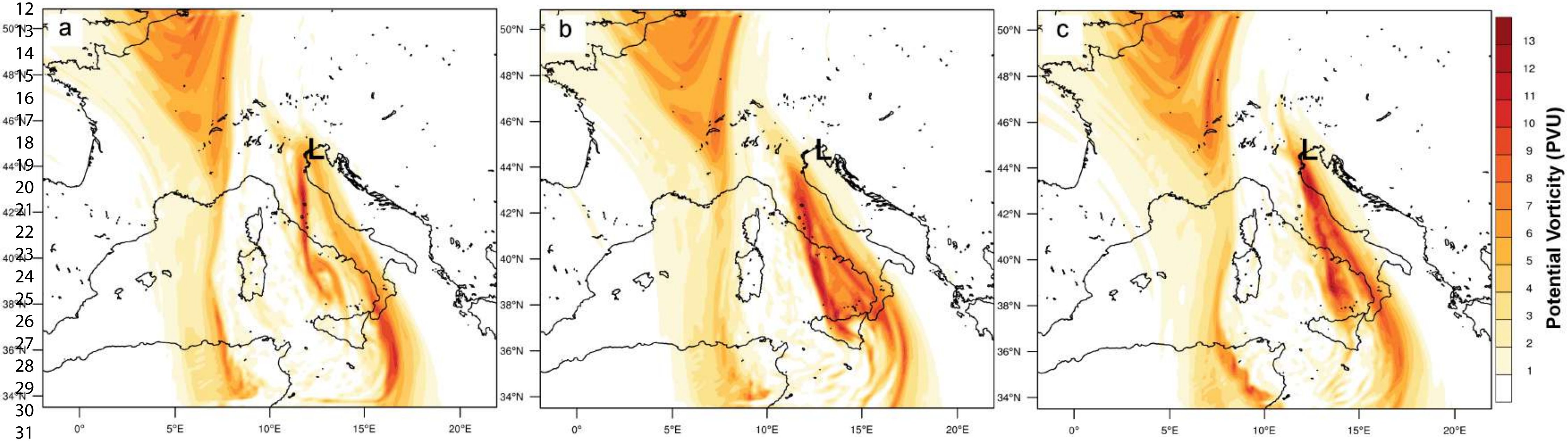
a
b
c
L
50°N
48°N
46°N
44°N
42°N
40°N
38°N
36°N
34°N
0°
5°E
10°E
15°E
20°E
Potential Vorticity (PVU)
1
2
3
4
5
6
7
8
9
10
11
12
13

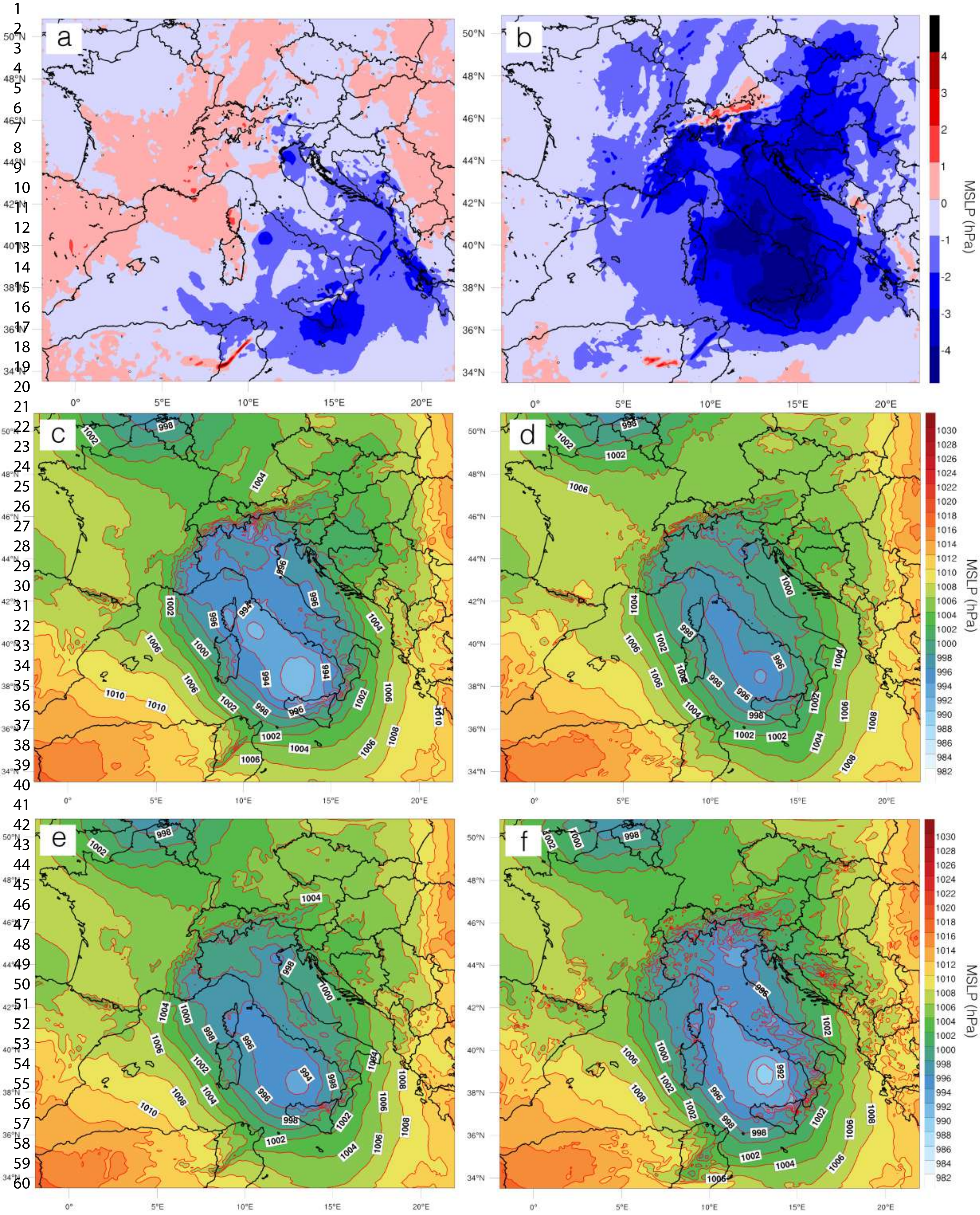
a
b
c
d
e
f
MSLP (hPa)
MSLP (hPa)
MSLP (hPa)
50°N
48°N
46°N
44°N
42°N
40°N
38°N
36°N
34°N
0°
5°E
10°E
15°E
20°E
4
3
2
1
0
-1
-2
-3
-4
1030
1028
1026
1024
1022
1020
1018
1016
1014
1012
1010
1008
1006
1004
1002
1000
998
996
994
992
990
988
986
984
982

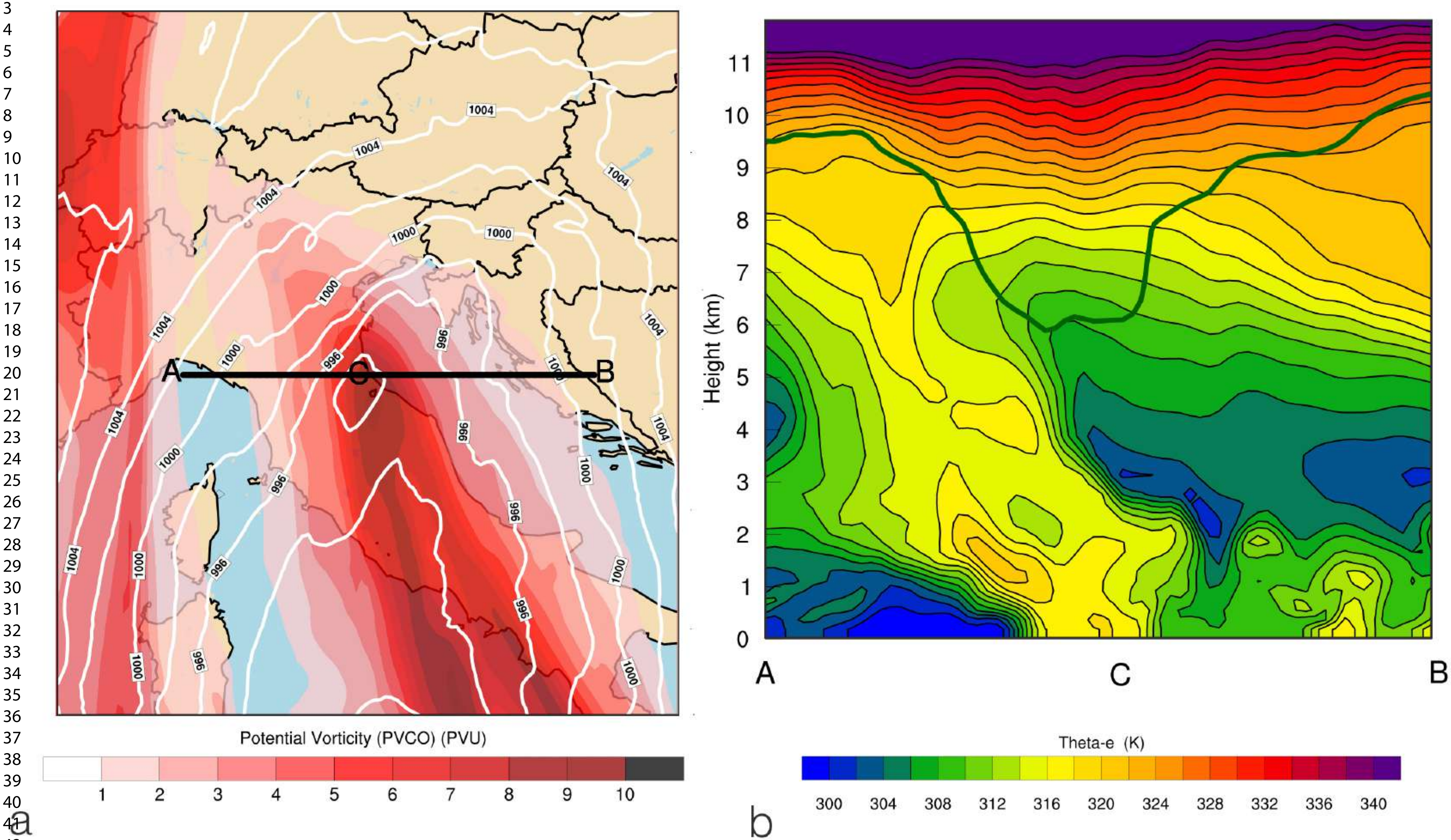
A
C
B
1004
1000
996
Potential Vorticity (PVCO) (PVU)
1 2 3 4 5 6 7 8 9 10
a
Height (km)
0 1 2 3 4 5 6 7 8 9 10 11
A
C
B
Theta-e (K)
300 304 308 312 316 320 324 328 332 336 340
b

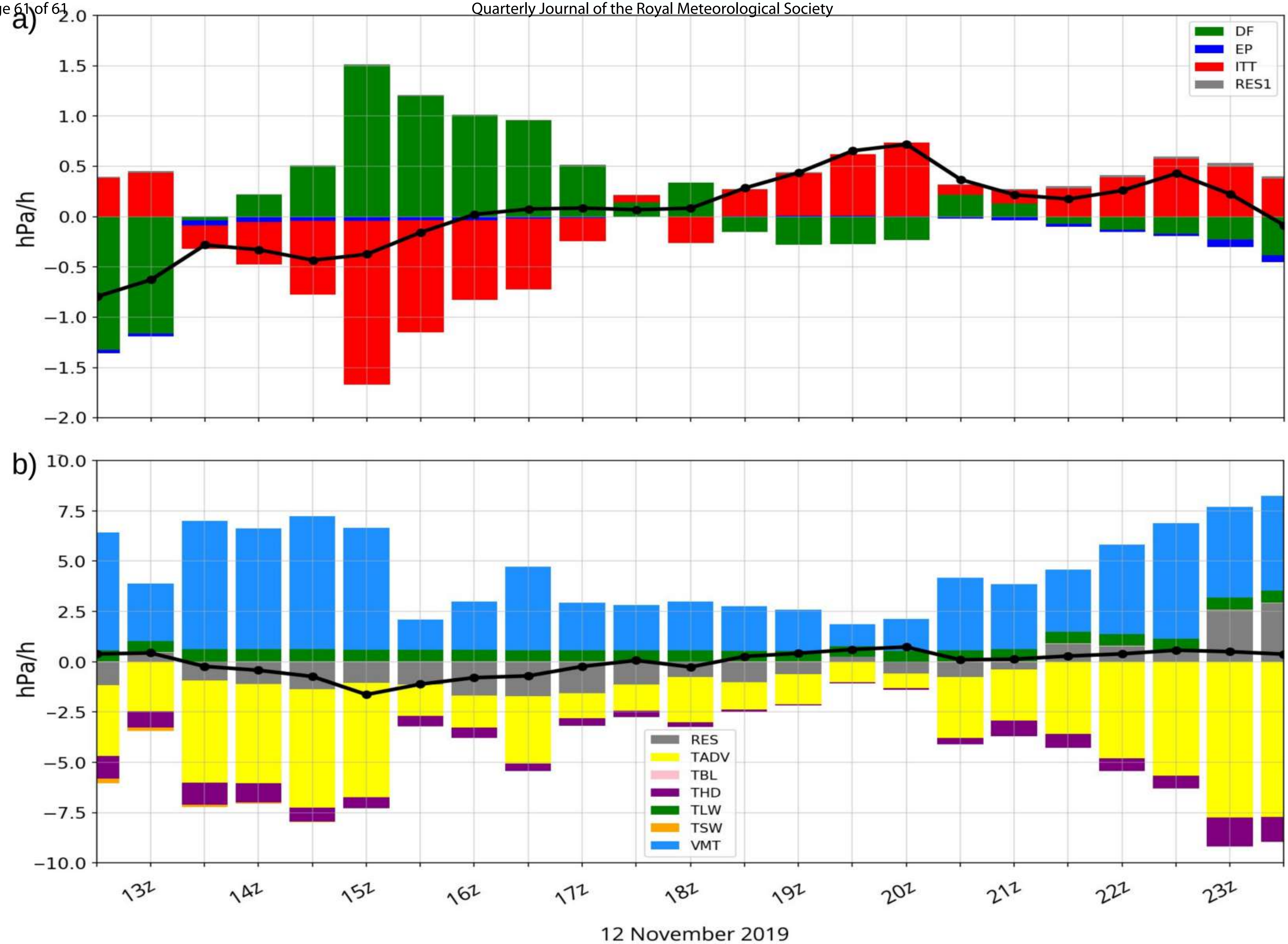
a)
2.0
1.5
1.0
0.5
0.0
−0.5
−1.0
−1.5
−2.0
hPa/h
DF
EP
ITT
RES1
b)
10.0
7.5
5.0
2.5
0.0
−2.5
−5.0
−7.5
−10.0
hPa/h
RES
TADV
TBL
THD
TLW
TSW
VMT
13z
14z
15z
16z
17z
18z
19z
20z
21z
22z
23z
12 November 2019